




Mid-Miocene silicic explosive volcanism of the Tokaj Mts., eastern-central Europe: eruption chronology, geochemical fingerprints and petrogenesis

Journal Article

Author(s):

Lukács, Réka; [Guillong, Marcel](#) ; Szepesi, János; [Szymanowski, Dawid](#) ; Portnyagin, Maxim; Józsa, Sándor; Bachmann, Olivier; Petrelli, Maurizio; Müller, Samuel; Schiller, David; Fodor, László; [Chelle-Michou, Cyril](#) ; Harangi, Szabolcs

Publication date:

2024-06

Permanent link:

<https://doi.org/10.3929/ethz-b-000656688>

Rights / license:

[Creative Commons Attribution 4.0 International](#)

Originally published in:

Gondwana Research 130, <https://doi.org/10.1016/j.gr.2024.01.004>



Contents lists available at ScienceDirect

Gondwana Research

journal homepage: www.elsevier.com/locate/gr

Mid-Miocene silicic explosive volcanism of the Tokaj Mts., eastern-central Europe: Eruption chronology, geochemical fingerprints and petrogenesis

Réka Lukács^{a,b,*}, Marcel Guillong^c, János Szepesi^{b,d}, Dawid Szymanowski^c, Maxim Portnyagin^e, Sándor Józsa^f, Olivier Bachmann^c, Maurizio Petrelli^g, Samuel Müller^{h,1}, David Schillerⁱ, László Fodor^{j,k}, Cyril Chelle-Michou^c, Szabolcs Harangi^{b,f}

^a Institute for Geological and Geochemical Research, HUN-REN Research Centre for Astronomy and Earth Sciences (MTA Centre of Excellence), Budapest, Budaörsi út 45 H-1122, Hungary

^b HUN-REN-ELTE Volcanology Research Group, Pázmány P. sétány 1/C 1117, Budapest, Hungary

^c Institute of Geochemistry and Petrology, Department of Earth Sciences, ETH Zürich, Clausiusstrasse 25 8092, Zürich, Switzerland

^d HUN-REN Institute for Nuclear Research, Bem tér 18/c 4026, Debrecen, Hungary

^e GEOMAR Helmholtz Centre for Ocean Research Kiel, Wischhofstr. 1-3 24148, Kiel, Germany

^f ELTE Eötvös Loránd University, Institute of Geography and Earth Sciences, Department of Petrology and Geochemistry, Pázmány P. s. 1/C 1117, Budapest, Hungary

^g Department of Physics and Geology University of Perugia, Piazza Università, 06100, Perugia, Italy

^h Institute of Geosciences, Kiel University, Ludewig-Meyn-Strasse 10 24118, Kiel, Germany

ⁱ Department of Chemistry and Physics of Materials, University of Salzburg, Jakob Haringer Straße 2a A-5020, Salzburg, Austria

^j HUN-REN Institute of Earth Physics and Space Science, Csatkai E. u. 6-8 9400, Sopron, Hungary

^k ELTE Eötvös Loránd University, Institute of Geography and Earth Sciences, Department of Geology, Pázmány P. s. 1/C 1117, Budapest, Hungary

ARTICLE INFO

Article history:

Received 17 July 2023

Revised 11 December 2023

Accepted 14 January 2024

Available online 22 January 2024

Handling Editor: A. Festa

Keywords:

Pyroclastic rock

Ignimbrite

Zircon petrochronology

Crystal-poor rhyolite

Caldera-forming eruption

Syn-extensional volcanism

ABSTRACT

The Tokaj Mts. volcanism occurred in a thinning continental lithosphere regime at the final stage of the subduction process. Using high-precision zircon U-Pb dating, four major explosive eruption events were distinguished. Among them the 13.1 Ma Sátoraljaújhely and the 12.0 Ma Szerencs eruptions could have yielded large amount of volcanic material (possibly > 100 km³) and they were associated with caldera collapse as shown by the several hundred-metre-thick pyroclastic deposits and the long (>100 km) run-out pyroclastic flow in case of the 13.1 Ma eruption. The 12.3 Ma Hegyköz and the 11.6 Ma Vizsoly eruptions were relatively smaller. The volcanic products can be readily distinguished by zircon and glass trace elements and trace element ratios, which can be used for fingerprinting and to correlate with distal deposits. The Rb, Ba, Sr content and strong negative Eu-anomaly of the glasses reflect extreme crystal fractionation, particularly for the Szerencs rhyolitic magma. The silicic volcanic products of the Tokaj Mts. show compositional similarities with the so-called 'dry-reduced-hot' rhyolite type consistent with an origin in an extensional environment, where the primary magmas were formed by near-adiabatic decompression melting in the mantle with subordinate fluid flux. In contrast, some of the older Bükkalja rhyolitic magmas evolved via more hydrous evolutionary paths, where amphibole played a role in the control of the trace element budget. The significant increase of zircon ϵ_{Hf} values from -8.8 to $+0.2$ in the rhyolitic pyroclastic rocks of Tokaj Mts. with time implies that mantle-derived magmas became more dominant. This can be explained by the specific tectonic setting, i.e. the final stage of subduction when the descending subducted slab became almost vertical, which exerted a pull in the upper lithosphere leading to thinning and accelerated subsidence as well as asthenospheric mantle flow just before the slab detachment.

© 2024 International Association for Gondwana Research. Published by Elsevier B.V. All rights reserved.

* Corresponding author.

E-mail addresses: lukacs.reka@csfk.org (R. Lukács), marcel.guillong@erdw.ethz.ch (M. Guillong), dawid.szymanowski@erdw.ethz.ch (D. Szymanowski), jozsa.sandor@ttk.elte.hu (S. Józsa), olivier.bachmann@erdw.ethz.ch (O. Bachmann), maurizio.petrelli@unipg.it (M. Petrelli), samuel.mueller@mpa.uni-stuttgart.de (S. Müller), DavidSchill3-r@aol.de (D. Schiller), fodor.laszlo@epss.hun-ren.hu (L. Fodor), cyril.chelle-michou@erdw.ethz.ch (C. Chelle-Michou), harangi.szabolcs@ttk.elte.hu (S. Harangi).

¹ presently at Material Testing Institute, University of Stuttgart, Pfaffenwaldring 4c, 70569 Stuttgart, Germany.

<https://doi.org/10.1016/j.gr.2024.01.004>

1342-937X/© 2024 International Association for Gondwana Research. Published by Elsevier B.V. All rights reserved.

1. Introduction

Very large or even supersized eruptions have received significant attention in the last two decades (Mason et al., 2004; Sparks et al., 2005; Self, 2006; Bachmann and Bergantz, 2008; Brown et al., 2014; Wilson et al., 2021; Zalinge et al., 2022) as they represent some of the most destructive events in our planet (Woo, 1999; Papale and Marzocchi, 2019). On the other hand, they also have positive outcomes, producing fertile soils, and helping to concentrate key metals and rare elements in shallow crustal level. Such large volcanic events, typically generating calderas upon eruption, can occur in different tectonic settings (mostly subduction zones, but also intraplate areas; e.g., Hildreth, 1981; Christiansen, 1984; de Silva, 1989; Christiansen et al., 2002; Bachmann and Bergantz, 2008; Rowland et al., 2010; Hughes and Mahood, 2011). Although the crystal mush model (Hildreth, 2004; Bachmann and Bergantz, 2004; Bachmann and Huber, 2016) offers an explanation for the formation of crystal-poor and crystal-rich eruptive products, there is no generalized, single model for the massive accumulation of magmas in the upper crust and extraction of melt-dominated body from the crystal mush (Wilson et al., 2021).

The largest volcanic eruptions in Europe for the last 20 Myr are considered to have occurred in the Pannonian Basin during an ignimbrite flare-up episode coeval with lithospheric extension between 18.1 Ma and 14.4 Ma (Lukács et al., 2018). This suggestion was recently supported by new results showing that silicic pyroclastic deposits in the nearby areas, in Austria, Croatia and Romania, can be correlated with the explosive eruption episodes at 18.1 Ma, 17.3 Ma and 14.4 Ma (Bercea et al., 2023; Brlek et al., 2023; Šegvić et al., 2023). Furthermore, Brlek et al. (2023) pointed out that pyroclastic flows during these eruptions could have a long runout (>100 km), which can be related to large, caldera-forming eruptions. Karátson et al. (2022) also emphasized the large size of the 17.3 Ma eruption, estimating at least VEI (Volcanic Explosivity Index) 7 scale. Major part of the volcanic products is buried by young sediments, however, drillings revealed several hundred metre, even > 1000 m thick pyroclastic deposits in the basement of the Great Hungarian Plain (Pantó, 1963; Széky-Fux and Kozák, 1984). Following the major ignimbrite flare-up event, silicic volcanism continued eastwards as shown by the bimodal andesitic-rhyolitic volcanism of the Tokaj Mts., NE Pannonian basin, where massive crystal-poor ignimbrite sheets were described (Pantó, 1962, 1963). Although they are usually thoroughly altered, zircon as a resistant mineral phase can provide valuable information about the magma genesis as well as the eruption ages. Combining zircon U–Pb dates, Lu–Hf isotope and trace element compositions with bulk rock and in-situ glass shard trace element data, we explore further the role, the size and the origin of the silicic explosive volcanic events in the Pannonian Basin during the Middle to Late Miocene (i.e. after 14 Ma) and attempt to explain this activity in the context of the geodynamic setting.

2. Geological background

2.1. Neogene to Quaternary geodynamic evolution and volcanism of the Carpathian–Pannonian Region

The Carpathian–Pannonian Region (CPR) in eastern–central Europe comprises an interarc extensional basin system (Pannonian Basin) surrounded by orogenic belts (Alps, Carpathians, Dinarides) typical in the Mediterranean area (Horvath et al., 1981, 2006, 2015; Bada et al., 2007; Schmid et al., 2008; Handy et al., 2015; Fig. 1). The Pannonian Basin is underlain by two microplates (called ALCAPA and Tisza–Dacia), which have different pre-Miocene histories (Balla, 1984; Csontos et al., 1992). The compressional orogenic

regime in the Alps resulted in the lateral extrusion of the ALCAPA unit eastward during the late Palaeogene–Early Miocene (Kázmér and Kovács, 1985; Ratschbacher et al., 1991a; 1991b; Csontos et al., 1992; Ustaszewski et al., 2008), where it was juxtaposed with the Tisza–Dacia unit and moved further together, presumably enhanced by a retreating subduction along the Northeast–East Carpathians (Royden et al., 1982, 1983; Balla, 1984; Csontos et al., 1992; Tari et al., 1992, 1999; Horváth, 1993; Csontos, 1995; Fodor et al., 1999; Horváth et al., 2006, 2015). Tectonic movement occurred along a dextral transpressional fault zone (Csontos and Nagymarosy, 1998; Fodor et al., 1998), called the Mid-Hungarian Shear Zone, which separates the two microplates. The lateral extrusion of the ALCAPA was accompanied by core-complex type extension (Tari et al., 1992, 1999) connected to the formation of several extensional subbasins by significant continental lithosphere thinning in both microplates (e.g., Styrian basin, Danube basin, Drava trough, Makó and Békés trough, East Slovakian–Transcarpathian basin; Horváth et al., 2015; Balázs et al., 2016; Tari et al., 2021). The onset and the major phase of extensional tectonics and sedimentation was diachronous across the Pannonian Basin, starting at ~ 25–23 Ma in the southern and western parts, and lasting as late as ~ 10–9 Ma in the eastern parts (Ustaszewski et al., 2010; Maţenco and Radivojević, 2012; Balázs et al., 2016; Fodor et al., 2021). The postulated subduction was terminated at around 9–11 Ma, when shortening along the Outer Carpathians stopped (Nakapelyukh et al., 2018). The extensional phase was followed by major post-rift subsidence and later by neotectonic inversion (Horváth and Cloetingh, 1996; Fodor et al., 2005; Dombrádi et al., 2010; Horváth et al., 2015).

This complex tectonic evolution was associated with widespread volcanic activity in the CPR fed by variable magmas for the last 20 Myr (Szabó et al., 1992; Seghedi et al., 1998; 2004, 2005; Harangi, 2001; Harangi et al., 2001, 2007, 2015; Konečný et al., 2002; Harangi and Lenkey, 2007; Seghedi and Downes, 2011; Lukács et al., 2018; Brlek et al., 2023; Fig. 1). The volcanism commenced with dominantly silicic explosive eruptions during the *syn*-rift phase between 18.1 and 14.4 Ma (Lukács et al., 2015, 2018, Brlek et al., 2023), although coeval andesitic and dacitic volcanic activity in the interior of the Pannonian Basin was also reported from boreholes. The silicic volcanism is considered to have been the most volumetrically significant event in Europe in the last 20 Myr, yielding a total of > 4000 km³ tephra. Distal pyroclastic deposits have been revealed at > 500–1000 km distance and they can be correlated to the main eruption events in the Pannonian Basin based on combined zircon age and trace element data (e.g. Arp et al., 2021; Brlek et al., 2023; Šegvić et al., 2023; Bercea et al., 2023). This volcanism was partly contemporaneous with the formation of complex andesitic–dacitic and andesitic–rhyolitic volcanic areas (stratovolcanoes and lava dome fields) having calc-alkaline chemical character between 16 and 9 Ma in the northern part of the Pannonian Basin (e.g., Pécskay et al., 2006; Harangi et al., 2007). The latest volcanic activity (11–0.1 Ma) in the CPR is characterised by the development of a post-collisional andesitic to dacitic volcanic chain in the East Carpathians (Seghedi et al., 2011, 2019, 2023), sporadic eruptions of ultrapotassic magmas (Harangi et al., 1995; Seghedi et al., 2008) and formation of alkaline basalt monogenetic volcanic fields (Harangi et al., 2015).

2.2. Structural setting of the Tokaj–Slanské vrchy Mts.

The Tokaj–Slanské vrchy Mts. (TSM; Fig. 1) is located in the northeastern part of the CPR close to the Carpathian orogenic belt (Kováč et al., 2007; Vass, 1998), and record a considerable part of the Miocene intermediate andesitic to rhyolitic volcanism (Gyarmati, 1977; Kaličiak and Žec, 1995; Zelenka et al., 2012). The area comprises a series of north–south trending volcanic complexes, around 100 km length and 15–25 km width extending obli-

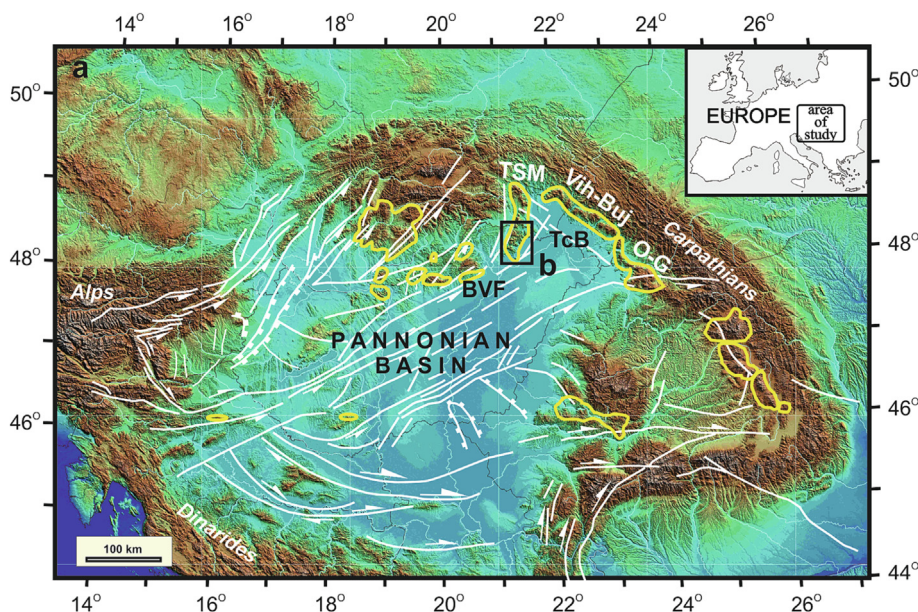


Fig. 1. (a) Location of the Tokaj–Slanské vrchy Mts. (TSM) in the Carpathian–Pannonian Region. Yellow lines delineate the Miocene to Quaternary calc-alkaline intermediate to silicic volcanic complexes on the surface. BVF: Bükkalja volcanic field (Lukács et al., 2018); TcB: Transcarpathian Basin; Vih-Buj: Vihorlat-Bujora volcanic chain (Outer Arc; Seghedi et al., 2001); O-G: Oas-Gutai Mts.; LD: Lénárdaróc locality. (b) Simplified geological map of the Tokaj Mts. (southern part of the Tokaj-Slanské vrchy Mts., yellow line delineates the Hungarian-Slovakian state boundary) modified after Gyarmati et al. (1976). (For interpretation of the references to colour in this figure legend, the reader is referred to the web version of this article.)

quely to the strike of the Carpathian orogenic structures. Its northern, Slovakian part is called Slanské vrchy Mts., while the southern, Hungarian part takes the name Tokaj Mts. (TM). The magmatic rocks of the TSM developed at the western margin of the Transcarpathian basin (TcB, after Kováč et al., 1995; Soták et al., 2000; Seghedi and Downes, 2011), a deep sedimentary basin at the junction of the ALCAPA microplate with Tisza-Dacia, spreading parallel to the Carpathians. The TcB is bordered by a poorly constrained hypothetical N-S striking fault system (Hernád–Hornád fault) from the west, and the E–W–striking Bogdan–Dragos–Vodá fault zone as the continuation of the Mid-Hungarian Shear Zone from the south. The TM is bounded on the east by the Ronyva fault, whose elevated footwall, composed of pre-Cenozoic formations (Zemplínské vrchy Mts.), represents and intra-basin height within the TcB (Fig. 1B).

The several km thick sedimentary pile within the TcB also contains multiple volcanic formations. Volcanic eruptions products are well-preserved along the margins of the TcB (Baráth et al., 1997) and built up chains of composite volcanoes, namely the TSM at the west, the Vihorlat-Bujora at the east and the Oas-Gutai volcanic range at the southeast borders (e.g. Kaličiak and Žec, 1995; Lexa et al., 2010; Seghedi and Downes, 2011; Seghedi et al., 2013; Zelenka et al., 2012; Kovacs et al., 2017). Remarkably, the Vihorlat-Bujora volcanic chain, called the Outer arc by Seghedi et al. (2001), developed right on the boundary zone between the ALCAPA unit and the thin-skinned fold-and-thrust belt of the Outer Carpathians, the accretionary prism between the converging plates. Volcanism along the Outer arc occurred between 13.8 Ma and 9.1 Ma (Pécskay et al., 2000, 2006), roughly contemporaneously with the volcanic activity of the TSM. The TSM, particularly their southern segment (TM), is underlain by a relatively thin crust (25–27 km; Lenkey et al., 2002; Horváth et al., 2015; Kalmár et al., 2021) and lithosphere (around 80 km; Horváth, 1993; Horváth et al., 2006; Kalmár et al., 2023) which is associated with a relatively high heat-flow (>100 mW/m²; Dövényi and Horváth, 1988; Lenkey et al., 2002; Horváth et al., 2015). This tectonic setting is related to the evolution of the CPR and particularly to the formation of the extensional Pannonian Basin.

2.3. Volcanism of the Tokaj Mts.

In this paper we focus on the southern segment of the TSM, i.e. the Tokaj Mts. (TM), where vast amount of silicic pyroclastic rocks occurs (Fig. 1). The TM is characterized by dominantly andesitic and rhyolitic volcanism with subordinate amount of dacites and only one locality of basalt (Gyarmati, 1977; Salters et al., 1988; Downes et al., 1995; Kiss et al., 2010; Lexa et al., 2014). Results of extensive K/Ar studies imply that eruptions occurred for a prolonged period, between ~ 15 and ~ 9 Ma (from 14.6 ± 0.8 to 9.4 ± 0.5 Ma, Pécskay et al., 1987, 1995, 2006; 15.2 – 9.4 Ma, Pécskay and Molnár, 2002). Pantó (1961, 1962) recognized and described ignimbrites in the TM and provided a classification scheme of various ignimbrite types among the first in the international literature. A palaeovolcanic reconstruction using volcanological, petrological, geochemical and geophysical results was given by Zelenka et al. (2012), who also outlined the potential locations of calderas. Deposition occurred initially partly in a shallow marine environment (Gyarmati, 1977; Szentgyörgyi, 1978; Kováč et al., 2007, 2018; Piller et al., 2007) shown by hyaloclastites, peperites and soft-sediment deformations (Németh et al., 2008), while later eruptions took place mostly in subaerial conditions.

Within the TM, four silicic explosive volcanoclastic units can be distinguished (Fig. 2). The oldest volcanic rocks in the TM are pyroclastic, called hereafter Sátoraljaújhely (SAU) Unit. This comprises massive and stratified lapilli tuffs, tuffites of rhyolitic to rhyodacitic composition. They were deposited either directly on the pre-Cenozoic basement (eastern part) or are intercalated within the Badenian marine sedimentary succession (Fig. 2). Surface occurrence is confined to the eastern part of the TM (Fig. 1), where borehole data indicate thickness exceeding 300 m (in places up to 600 m). The thick pile of pyroclastic rocks was mostly described as upper Badenian, however, their K–Ar ages vary between 15.2 ± 0.6 Ma and 13.1 ± 0.5 Ma (Pécskay et al., 1987, Pécskay and Molnár, 2002). Most of the SAU volcanic rocks are hydrothermally altered (argillization, silicification dated by the K–Ar method to ~ 13.2 – 13.0 Ma; Pécskay and Molnár, 2002), glass shards were replaced in the submarine environment by secondary

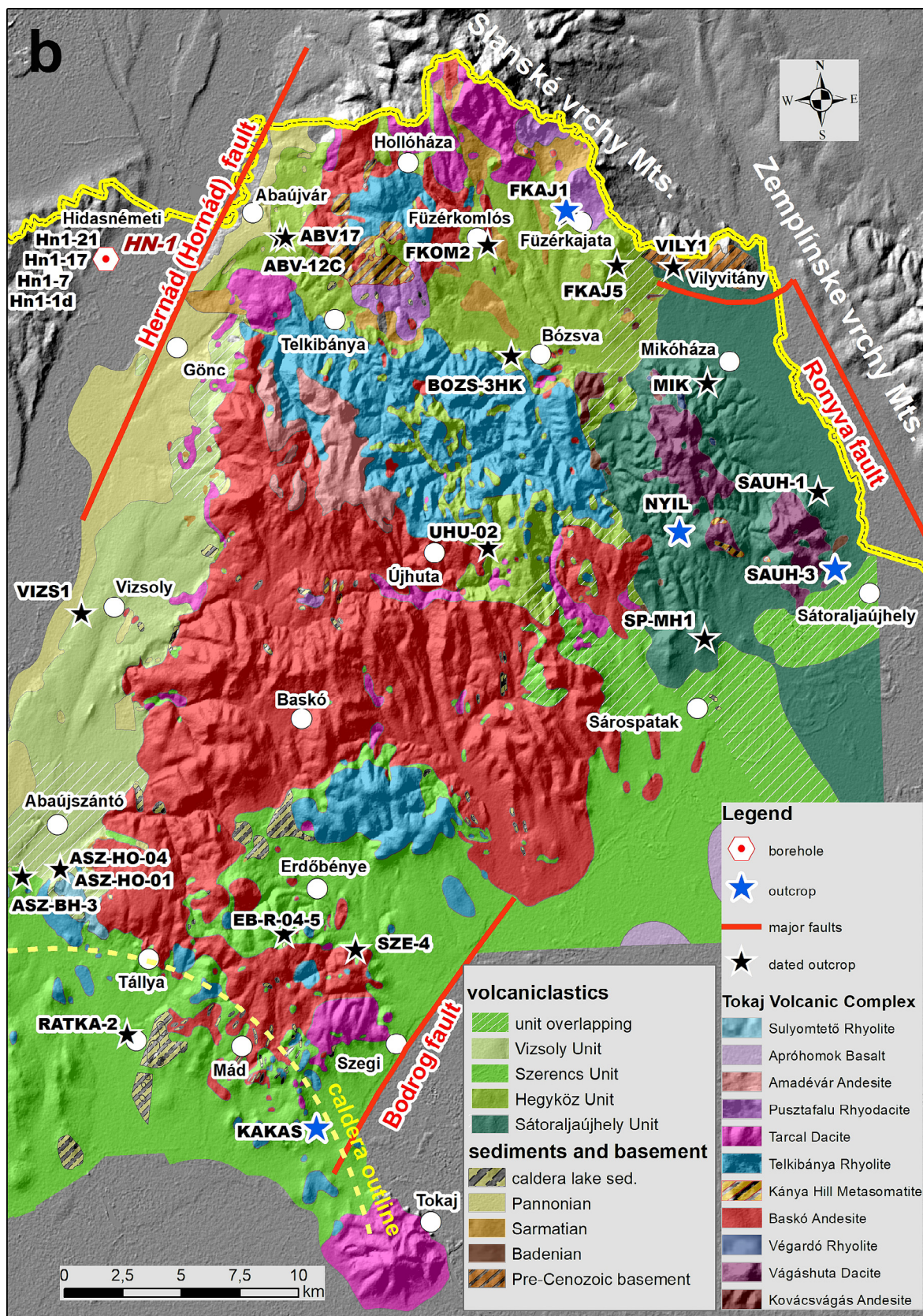


Fig. 1 (continued)

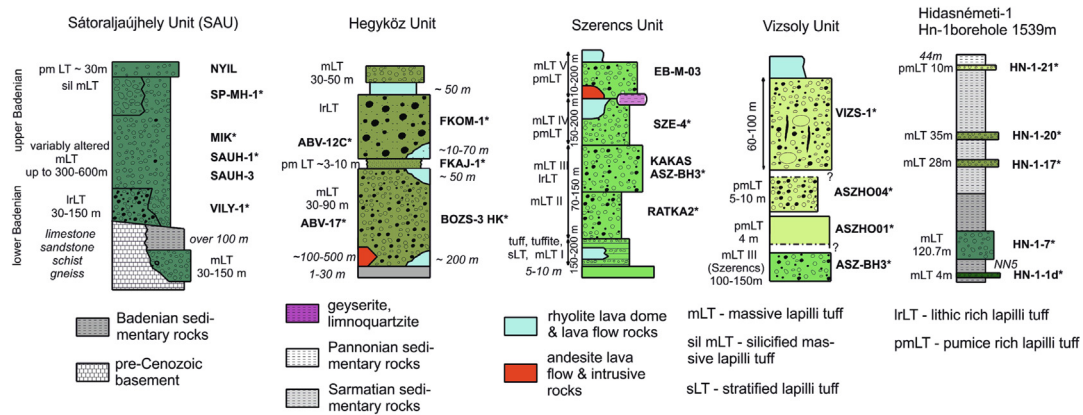


Fig. 2. Simplified stratigraphic sections of the distinguished explosive silicic eruptive units with the positions of the collected samples.

minerals such as zeolites and phyllosilicates. Several subunits were distinguished within the SAU representing different volcanological facies formed from consecutive eruptions: zeolitized and silicified ignimbrite, fall and ash flow tuff, redeposited tuff-tuffite and a slightly less silicic rhyodacitic subunit found only in one borehole (Fig. 2). Associated rhyolitic and dacitic lava domes as well as andesitic lavas postdate this pyroclastic succession (e.g. Pécskay and Molnár, 2002; Zelenka et al., 2012).

Another major explosive eruption phase occurring in the Sarmatian (K-Ar dating suggests ages from 12.4 ± 0.8 to 11.7 ± 0.5 Ma; Pécskay et al., 1987) resulted in various pyroclastic flow deposits (ignimbrites, dome-related block and ash flow deposits; Szepesi et al., 2019; Fig. 2). These are collectively called as Hegyköz Unit (Gyarmati, 1977), which is confined mostly in the northern part of the TM. The thickness of the Hegyköz succession is ~ 100 – 150 m including rhyolitic lava intercalations (Szepesi et al., 2019). The explosive volcanism was followed again by andesitic and rhyolitic effusive volcanic activity.

In the southern part of the TM, silicic pyroclastic rocks were described as deposits of the Szerencs succession (Zelenka, 1964), here referred as the Szerencs Unit (Fig. 1). It is a 200–350 m thick series of volcanoclastic deposits intercalated with redeposited tuff, tuffite and argillaceous sediments and in some places with rhyolitic and andesitic lavas (Fig. 2). Zelenka (1964) identified five eruption subunits in borehole and outcrop successions that were deposited partly in subaqueous and partly in subaerial environments (Fig. 2). Local palaeotopographic changes, facies and secondary alteration (zeolitization and hydrothermal processes) make it difficult to determine the thickness and to separate the different units; however, according to Zelenka (1964) the thickness of single eruption units varies between 70 and 250 m (Fig. 1). The pyroclastic rocks of the Szerencs Unit are typically crystal-poor (mostly ~ 5 – 10 %) and appear to show a gradual increase in SiO_2 and K_2O upwards. The Celebration-4 (CEL-4) deep seismic profile (Hegedűs et al., 2002) and a magnetic gradient map (Zelenka et al., 2012) identified a ring-shaped caldera-like structure ca. 25 km in diameter in the southwest part of the TM, which can be considered the source of this volcanic succession. The caldera rim is marked by a series of associated rhyolitic-andesitic lava domes and subvolcanic bodies (Zelenka et al., 2012). K-Ar ages related to the Szerencs Unit (including lavas) yielded 12.2 ± 0.5 to 11.3 ± 0.5 Ma (Pécskay and Molnár, 2002). Intensive hydrothermal activity and secondary alteration affected most of the rocks found on the surface (bentonite, diatomite, ore veins and lenses, kaolinite and alunite, dated to 12.4–10.4 Ma; Pécskay and Molnár, 2002).

Deposits of the youngest explosive eruption phase, denoted here as Vizsoly Unit, are confined to the western side of the TM and can be followed on the surface between Abaújszántó and

Gönc (Figs. 1, 2). It is dominantly built up by massive, pumice block-bearing lapilli tuffs that are in places rich in lithic (andesite, rhyolite) clasts. At Vizsoly, the several tens of metres thick, presumably valley-filling unwelded ignimbrite contains many gas-segregation pipes. The thickness of the formation is 50 m on average and exceeds 100 m in a few places. K-Ar dating suggests an age of 11.2 ± 0.5 Ma (Pécskay et al., 1987).

3. Samples and petrology

We studied 22 outcrops (Fig. 2) representing all the mapped silicic pyroclastic formations of the Tokaj Mts. in addition to cores of the borehole Hn-1 at the western margin of the TM (Fig. 1) and a single sample from Lénárddaróc. The main petrological and volcanological characteristics of the studied samples from the four silicic pyroclastic units and the drill cores are given in the Supplementary Data, Table S1.

We collected samples from six outcrops of the SAU that represent different facies and stratigraphic levels as shown in Fig. 2. No fresh volcanic glass was found in the SAU samples. Phenocryst assemblage contains plagioclase, quartz, sanidine and biotite in variable amounts.

The Hegyköz Unit was studied and sampled in seven outcrops; the most complete section was recorded in the Abaújvár Kátyú valley (Figs. 1, 2). Here, two subunits were distinguished, (1) a lower, min. 30 m thick pumice-rich massive lapilli tuff with gas-segregation pipes (lower ignimbrite), and (2) an upper, diffusely bedded, ca. 30 m thick massive lapilli tuff series where erosional channels filled by abundant lithic clasts are common (Szepesi et al., 2019). They are separated by stratified and silicified tuff layers. The other outcrops of this unit likely represent parts of these two volcanoclastic subunits. Secondary alteration (argillization, silicification) is local and less common than in the SAU. The pumiceous pyroclastic rocks are phenocryst-poor, containing plagioclase, quartz \pm biotite and have mostly fresh glass shards.

The Szerencs Unit was studied in five outcrops (Fig. 2), which represent all of the distinguished five subunits (Zelenka, 1964) except for the lowest one. Fresh rock was only available in the 4th subunit (Fig. 2). The pyroclastic rocks are phenocryst-poor (<5 %) and contain quartz, sanidine and plagioclase phenocrysts.

Three outcrops related to the Vizsoly Unit were studied. The most typical appearance occurs in the abandoned quarry at Vizsoly and it is represented by the VIZS-1 sample. It contains plagioclase and orthopyroxene \pm clinopyroxene as phenocrysts (up to 10 vol%). A sequence of three pyroclastic subunits was described near Abaújszántó (Fig. 2), which shows two consecutive pyroclastic flow deposits represented by samples ASZ-HO01 and ASZ-HO04. They are discontinuously overlain by the typical ignimbrite of Vizsoly

Unit represented by the VIZS-1 sample (Fig. 2). The lower two sub-units differ in mineral composition from the VIZS-1 sample having quartz, plagioclase, biotite and sanidine as phenocrysts.

Additional samples from the Hidasnémeti-1 (Hn-1) borehole, located at the northwestern margin of the Tokaj Mts. (Fig. 1b) were included. They represent five well-recognizable volcanoclastic units of the 1539 m-long borehole section (Fig. 2; Bodor and Fodor, 2013). We studied samples from four of these beds. Furthermore, we sampled an outcrop, Kakarcsó Hill, Lénárddaróc (Fig. 1), located 100 km to northwest. The Lénárddaróc pyroclastic rocks (Fodor et al., 2005) were previously suggested to belong to the Harsány Formation (Lukács et al., 2022) based on the geochemical similarities with the 14.4 Ma Harsány ignimbrite (Lukács et al., 2015, 2018) of the Bükkalja volcanic field, although accurate zircon U-Pb dates were missing here. The outcrop shows a ~ 14 m thick section with two fine-grained lapilli tuff units (pumices < 3 cm) of pyroclastic flows separated by a cross-bedded undulating fine ash tuff (pyroclastic surge deposit). The lower unit commonly contains charcoal fragments (up to 20 cm), while the upper one (above the tuff bed) is an accretionary lapilli-bearing pyroclastic flow deposit with gas-segregation pipes (details are in Fodor et al., 2005; Lukács et al., 2022). They contain quartz, plagioclase, biotite and subordinate sanidine as phenocrysts (ca. 10 vol%) as well as fresh volcanic glass (glass shard, pumice).

4. Analytical methods

Analytical methods are given with more details in the [Supplementary Data](#), Sheet 1 and reference material data are provided in the [Supplementary Data](#), Table S2 and Table S3.

In situ zircon U-Pb isotopes, trace element contents and Lu-Hf isotopes were analysed at ETH Zürich. U-Pb isotopes were measured simultaneously with trace elements (from the same ablated volume) using a Thermo Element XR SF-ICP-MS coupled with a Resonetics Resolution 155 type ablation system. We used a 30 µm spot size, 5 Hz repetition rate, 2.0 J/cm² energy density (fluence) and 40 s ablation time. For U-Pb dating, GJ-1 reference zircon (Jackson et al., 2004; Horstwood et al., 2016) was used as a primary reference material, while zircons 91500, Plešovice, AUSZ7-1, AUSZ7-5, Rak-17, Temora2 and LG-0302 were measured as validation reference materials (Wiedenbeck et al., 1995; Sláma et al., 2008; Kennedy et al., 2014; von Quadt et al., 2016; Webb et al., 2020; Black et al., 2004; Gutiérrez et al., 2018, respectively), covering an age interval between 1063.5 Ma and 2.409 Ma. Validation reference materials were used to correct the matrix dependent age offsets (Sliwinski et al., 2017). Data reduction of all LA-ICP-MS measurements were done using IOLITE (Paton et al., 2011), in case of U-Pb dating combined with VizualAge (Petrus and Kamber, 2012). The Th disequilibrium correction was performed after alpha dose-correction (Sliwinski et al., 2017) assuming a constant Th/U partition coefficient ratio of 0.33 ± 0.06 (1σ ; Rubatto and Hermann, 2007) and using the equations of Schärer (1984). The in-situ dates were not corrected for common Pb contents; however, during data reduction, integration intervals were set to exclude the common Pb contaminated signal intervals and data were filtered according to their discordance ($[(^{207}\text{Pb}/^{235}\text{U Age}) - (^{206}\text{Pb}/^{238}\text{U Age})] / (^{207}\text{Pb}/^{235}\text{U Age}) < 10\%$). Average uncertainty of the individual zircon dates is 1.4 – 2.3 %. (2 SE). For in-situ zircon trace element analysis we used NIST612 as primary reference material and zircon 91,500 and an in-house Synthetic Zircon Blank for quality control. Target elements were Si (internal standard), Zr, REE, Y, Hf, P, Nb, Ta, U, Th, Ti (see [Supplementary Data](#), Table S2), and either Al or Ba were measured for monitoring glass, apatite inclusions. Cathodoluminescence images of zircon grains with analytical spots are presented in ESM_4.

Zircons from four key samples were also dated by chemical abrasion isotope dilution thermal ionisation mass spectrometry (CA-ID-TIMS) at ETH Zürich using a Triton Plus TIMS. Select grains, most of which were previously analysed by LA-ICP-MS, were extracted from zircon mounts and individually annealed and chemically abraded (after Mattinson, 2005). The crystals were spiked with the EARTHTIME ²⁰⁵Pb-²³³U-²³⁵U tracer solution (Condon et al., 2015; McLean et al., 2015) dissolved, and their purified U-Pb fractions were analysed following methods similar to those in Brlek et al. (2023). All ²⁰⁶Pb/²³⁸U dates were corrected for initial ²³⁰Th/²³⁸U disequilibrium using a fixed partition coefficient ratio derived from a compilation of natural and experimental data ($D_{\text{zircon}}^{\text{Th/U}}/D_{\text{melt}}^{\text{Th/U}} = 0.183 \pm 0.061$, 1σ) and assuming that variations in Th/U between zircons reflect changes in magma composition rather than in U/Th partitioning.

In-situ Lu-Hf isotopic analysis was performed using a Resolution 193 nm ArF laser ablation system coupled to a Nu2 multicollector inductively-coupled-plasma mass-spectrometer (MC-ICP-MS). Ablation was carried out with 50 µm spot size, 5 Hz laser pulse repetition rate and 4 J/cm² energy density. The accuracy and precision of the data obtained were monitored through the systematic measurements of the well characterized RM Mud Tank (0.282507; Woodhead and Hergt, 2005), 91,500 (0.282307; Wu et al., 2006), Temora (0.282680; Wu et al., 2006), and GHR1 (0.283050; Eddy et al., 2019). Initial ¹⁷⁶Hf/¹⁷⁷Hf ratios and εHf were calculated using the crystallization age of each sample, the decay constant of Söderlund et al. (2004) for ¹⁷⁶Lu ($1.867 \times 10^{-11} \text{ a}^{-1}$) and the CHUR parameters of Bouvier et al. (2008).

Bulk rock composition of pumices and pyroclastic rocks was determined at the Bureau Veritas Mineral Laboratories (ACME Labs; <https://www.acmelab.com/>) using ICP-OES and ICP-MS technique for major-minor and trace elements, respectively. Internal standards and duplicate sample analysis by sessions were used to check the reliability of the results.

Major and trace element composition of volcanic glass was analysed for each pyroclastic unit, except for SAU (where no fresh glasses were found) and from the Lénárddaróc outcrop. Major elements in 20–22 glass shards per sample were analysed at GEOMAR (Kiel, Germany) using JEOL JXA 8200 electron microprobe. The analytical conditions were 15 kV accelerating voltage, 6nA current and 5 µm electron beam size for all analyses. Full analytical details and data on long-term analytical precision can be found in Portnyagin et al. (2020).

Glass trace element analyses were obtained at the Institute of Geosciences, Christian-Albrecht University of Kiel (Kiel, Germany) using ICP-MS Agilent 8900 and a Coherent GeoLas ArF 193 nm Excimer LA system operated with a fluence of 5 J cm⁻², at a repetition rate of 10 Hz and 24 µm ablation craters. Ten major elements (Si, Ti, Al, Fe, Mn, Mg, Ca, Na, K, P) and 31 trace elements were analysed on typically 10–12 glass shards for every samples. Data reduction was performed in Glitter software (Griffin et al., 2008) that included manual selection of intervals for signal integration and preliminary calibration. The data was converted to concentrations by matching the sum of major element oxides to 100 wt% (e.g. Pettke et al., 2004). The calibration and correction of instrumental drift used data on ATHO-G reference glass (Jochum et al., 2006).

5. Results

5.1. LA-ICP-MS zircon U-Pb geochronology

The in-situ zircon U-Pb dating was performed on 23 samples during 7 analytical sessions (see data in [Supplementary Data](#), Table S2). Spot measurements (46–79 per sample) targeted mostly the outer parts of the zircon grains (here referred to as rim; see CL

images in [Supplementary Data](#), Sheet 2) and the analyses resulted in 71–93 % concordant data except for four samples, where only 41–57 % concordant data were obtained. Discordant dates were not corrected for common Pb and they were omitted from interpretation. Data with large uncertainties (>4% RSE) were also discarded. The majority of the zircon U-Pb dates vary between ~14.3 and 11.3 Ma, with only a few old xenocrystic dates found in four samples (~763–21.7 Ma, c.f. [Suppl. material](#)). Each sample has multicomponent age populations according to the calculated MSWD (Mean Squared Weighted Deviation) values of weighted mean ages, which have therefore no geologic meaning. Thus, we calculated the youngest population age (low-MSWD weighted mean) without the young outlier dates (suspected of Pb loss) for each sample and propagated an external uncertainty of 1.5 % representative of long-term reproducibility of RM data at the ETH LA-ICP-MS lab ([Sliwinski et al., 2022](#)). These youngest zircon crystallization ages are interpreted as the closest approximation of volcanic eruption ages. The youngest $^{206}\text{Pb}/^{238}\text{U}$ data populations based on the concordant dates cluster into four groups that are summarized in [Table 1](#).

The oldest samples of the TM belong to the SAU. All four samples have 1–2 measured spots giving xenocrystic dates (from ~763 to 21.6 Ma; see [Supplementary Data, Table S2](#)) and their spot dates range (without outliers) between 14.3 Ma and 12.8 Ma ([Fig. 3a](#)). The calculated youngest population ages are 13.2 ± 0.2 Ma to 13.1 ± 0.2 Ma. The second age group comprises eight samples from the Hegyköz Unit. The youngest population ages span 12.6 ± 0.2 Ma to 12.3 ± 0.2 Ma and the individual concordant rim dates vary between 13.8 Ma and 12.0 Ma ([Fig. 3b](#)). No xenocrystic spots were measured in these samples. The third age group is given by the four samples of the Szerencs Unit. They give very similar rim spot date ranges (12.9–11.7 Ma; without outliers) and identical, 12.0 ± 0.2 Ma youngest population ages ([Fig. 3c](#)). The youngest age group is represented by the three samples related to the Vizsoly Unit, which have overlapping youngest population ages of 11.6 ± 0.2 Ma to 11.7 ± 0.2 Ma ([Fig. 3d](#)). Individual rim spot dates range from 12.9 Ma to 11.2 Ma and only one old xenocrystic spot was measured (~326 Ma rim in ASZ_HO04; ~240 Ma core in Hn1-21).

The Lénárdaróc sample (LENDAR) belongs to the oldest age group as it gives overlapping date range (15.3 to 12.8 Ma) with the samples of SAU and within uncertainty give the same youngest population age (i.e. 13.05 ± 0.2 Ma; [Fig. 3a](#)). The four samples from Hn-1 borehole have distinct ages. The oldest sample (Hn1-1d) yielded 14.2 ± 0.2 Ma, which does not match any of the age groups defined above ([Fig. 3a](#)). This sample contains old xenocrystic grains with ages between 1.97 Ga and 364 Ma. Hn1-7 gives strikingly similar age to samples of the SAU. Dates span from 13.9 to 12.9 Ma and the youngest population age is 13.1 ± 0.2 Ma. Hn1-17 sample contains old (>Miocene age) and young, Miocene-aged grains. Half of the analyses were done in old grains which vary between 2.65 Ga and 247 Ma. The Miocene grains also returned a relatively large range of dates (17.9–12.15 Ma), the youngest population age based on eight spot dates is 12.4 ± 0.2 Ma. This age suggests a relation to the Hegyköz Unit. Sample Hn1-21 gives similar youngest population age to the Vizsoly Unit ([Fig. 3d](#)), which is 11.6 ± 0.2 Ma, and its date range (12.2–11.3 Ma) is similar with that recorded in the VIZS-1 sample (12.2–11.2 Ma). In Hn1-21, only one xenocrystic grain was measured (240 Ma core).

5.2. High-precision CA-ID-TIMS U-Pb geochronology

Five to six zircon crystals each from four samples representative of the four units distinguished by the LA-ICP-MS dates were also analysed by CA-ID-TIMS. Three samples (MIK, SZE-4, ABV-17) returned Th-corrected, single-crystal $^{206}\text{Pb}/^{238}\text{U}$ zircon dates that

were dispersed beyond analytical uncertainty; the fourth sample (VIZS1) contained unradiogenic zircons which returned six relatively imprecise and consequently indistinguishable dates ([Fig. 4](#)). We interpret these ranges to represent the (minimum) timescales of pre-eruptive zircon crystallisation within the feeding magma reservoir, with the youngest end of the population closely approximating the age of eruption. We used the obtained populations of single-crystal $^{206}\text{Pb}/^{238}\text{U}$ dates to obtain several alternative eruption age interpretations using 1) the youngest crystal age, 2) a Bayesian approach based on predictions of temporal distribution of zircon ages within a magma body ([Keller et al., 2018](#)), 3) a weighted mean for the case of the VIZS-1 ([Table 2](#) and [Fig. 4](#)). While all interpretations return overlapping ages, we suggest that given the small number of dates ($n = 5-6$) and the comparably low likelihood of Pb loss for these samples, the Bayesian approach is the least biased and thus offers the most robust age interpretation.

5.3. Zircon Lu-Hf isotopes and trace elements

The Lu-Hf isotopic composition of zircon from 5 representative samples from each eruption unit (MIK, ABV-17, FKOM-2, SZE-4, VIZS-1) as well as from the Hn1-1d drill core sample is given in [ESM_2](#). The ϵHf of studied zircons (40 spots/sample) were calculated using the obtained CA-ID-TIMS ages for the representative samples of the four units. The average uncertainty (given in 2SE) of single spot ϵHf values is around 2 units ($\pm 0.4\sigma$). Results show two distinct populations within the TM rhyolites based on ϵHf values, where the youngest two samples (SZE-4 and VIZS-1) yielded values between -1.8 and 2.5, while the other three samples from the older eruption units (MIK, ABV-17, FKOM-2) range from -10.5 to -3.9 ([Fig. 5](#)). Within the latter group the oldest sample (MIK) has systematically lower ϵHf values between -10.5 and -6.5, while the two samples representing the Hegyköz Unit have values above -8. Zircon from the Hn1-1d drill core sample has ϵHf values from -3.7 to 1.6 with a weighted mean of -0.9 ± 1.0 . These values show an overlap with those of the rhyolitic Harsány ignimbrite from the Bükkalja volcanic field ([Lukács et al., 2018](#); [Fig. 5](#)). Weighted mean of the ϵHf values (without some outliers; [Supplementary Data, Table S2](#)) for the TM rhyolites show gradual increase from MIK: -8.80 ± 0.54 , through ABV-17: -6.36 ± 0.63 and FKOM-2: -5.29 ± 0.61 to SZE-4: 0.14 ± 0.63 and VIZS-1: 0.19 ± 0.65 .

Trace element composition of the dated zircon grains shows a notable variation (data are available in [ESM_2](#)): they have Hf contents between 6576 and 16500 ppm, Ti is between 1 and 10 ppm, whereas Zr/Hf and Th/U ratios range between 28.9 and 77.4, and from 0.13 to 2.03, respectively ([Fig. 6](#)). U, Y and P contents yielded 56–5391 ppm, 408–7760 ppm and 189–4800 ppm ranges, respectively ([Fig. 6](#)). The U/Yb ratio values are between 0.3 and 4.0, which is typical for continental magmatic rocks ([Grimes et al., 2007](#); [2015](#)). Zircon Hf concentration data mostly negatively correlate with Th/U and with Ti contents ([Fig. 6](#)).

Samples belonging to the SAU show the largest variation in the Hf, Ti and P contents and in Th/U and Eu/Eu* (0.01–0.3) ratios ([Fig. 6](#)), while the largest variation in Nb content and Ce/Ce* (2–239) is represented by the samples of Szerencs Unit ([Fig. 6](#); Eu/Eu* and Ce/Ce* (after [Loader et al., 2017](#)) calculations are given in [Supplementary Data, Table S2](#)). Zircon spots belonging to the SAU and Vizsoly Units show relatively narrow and positive correlation trends on U versus Y diagram, while the Hegyköz Unit yielded the widest compositional range ([Fig. 6](#)). LENDAR zircon trace element data overlap and follow the trends of the SAU corresponding with their similar U-Pb dates. ASZ-HO01 and ASZ-HO04 zircon populations show similar chemical variations, although they are distinct from the VIZS-1 zircon grains, the latter having the lowest Hf contents ([Fig. 6](#)).

Table 1
Summary of the LA-ICP-MS dating results and the youngest population ages with uncertainties. Low-MSWD weighted mean is calculated using MSWD threshold values after [Wendt and Carl \(1991\)](#).

Unit	Locality	Sample name	Number of data/ concordant data	average uncertainty of dates	youngest population age ^a (Ma)	uncertainty (Ma)		number of data used	MSWD	Th/U	
				2SE in %		2SE ^b	2σ ^c			1SD	
Vizsoly Unit	Hn1_54.2–44.4 m	Hn1-21	59/40	1.72 %	11.60	0.04	0.18	22	1.5	0.64	0.14
	Vizsoly	VIZS1	65/27	2.31 %	11.56	0.08	0.19	18	1.7	0.80	0.30
	Abaújszántó	ASZ-H004	63/48	1.86 %	11.71	0.04	0.18	31	1.4	0.69	0.15
Szerencs Unit	Abaújszántó	ASZ-H001	79/66	1.85 %	11.70	0.03	0.18	51	1.3	0.61	0.17
	Rátka	RATKA-2	60/53	1.50 %	11.96	0.03	0.18	34	1.4	0.86	0.18
	Erdőbénye	EB-R-04–5	72/59	1.70 %	11.95	0.03	0.18	37	1.4	0.80	0.15
Hegyköz Unit	Szegi	SZE-4	46/38	1.41 %	12.00	0.05	0.19	22	1.6	0.81	0.12
	Abaújszántó	ASZ-BH-3	46/39	1.41 %	12.00	0.04	0.18	27	1.6	0.80	0.19
	Abaújvár valley	ABV-12C	50/40	1.74 %	12.57	0.04	0.19	27	1.4	0.65	0.26
Sátoraljaújhely Unit	Abaújvár valley	ABV17	50/42	1.78 %	12.62	0.04	0.19	36	1.3	0.70	0.33
	Nagybózsza	BOZS-3HK	77/55	1.73 %	12.50	0.03	0.19	38	1.4	0.70	0.31
	Füzérkajata	FKAJ1	56/47	1.81 %	12.63	0.05	0.19	37	1.5	0.69	0.26
	Füzérkajata	FKAJ5	50/39	1.61 %	12.49	0.04	0.19	27	1.3	0.64	0.27
	Füzérkomlós	FKOM2	64/57	1.73 %	12.39	0.05	0.19	29	1.6	0.65	0.18
	Újhuta	UHU-02	56/28	1.71 %	12.28	0.07	0.20	17	1.7	0.94	0.36
Sátoraljaújhely Unit	Hn1_662.8–659.7 m	Hn1-17	50/46	1.58 %	12.38	0.07	0.20	8	1.9	0.63	0.25
	Mikóháza	MIK	60/43	1.84 %	13.17	0.07	0.21	18	1.7	0.70	0.46
	Sátoraljaújhely	SAUH	50/27	2.04 %	13.24	0.06	0.21	18	1.4	0.76	0.38
	Vilyvitány	VILY-1	60/46	2.00 %	13.10	0.07	0.21	18	1.7	0.60	0.42
	Megyer-hill	SP-MH1	61/57	1.86 %	13.20	0.04	0.20	40	1.4	0.61	0.50
Harsány Unit	Hn1_1483.7–1405.5 m	Hn1-7	50/38	1.44 %	13.11	0.05	0.20	27	1.5	0.84	0.29
	Lénárdaróc	LENDAR	78/57	2.00 %	13.05	0.05	0.20	35	1.5	0.71	0.41
	Hn1_1538.2–1534.2 m	Hn1-1d	50/43	1.56 %	14.24	0.06	0.22	21	1.7	0.57	0.14

^a low-MSWD weighted mean.

^b weighted mean age uncertainty; ^cpropagated uncertainty is calculated by quadratic adding of uncertainty of ages and 1.5 % external error of LA-ICP-MS measurements; SE = Standard Error, σ = szigma, SD = Standard Deviation, MSWD = Mean Standard Weighted Deviation

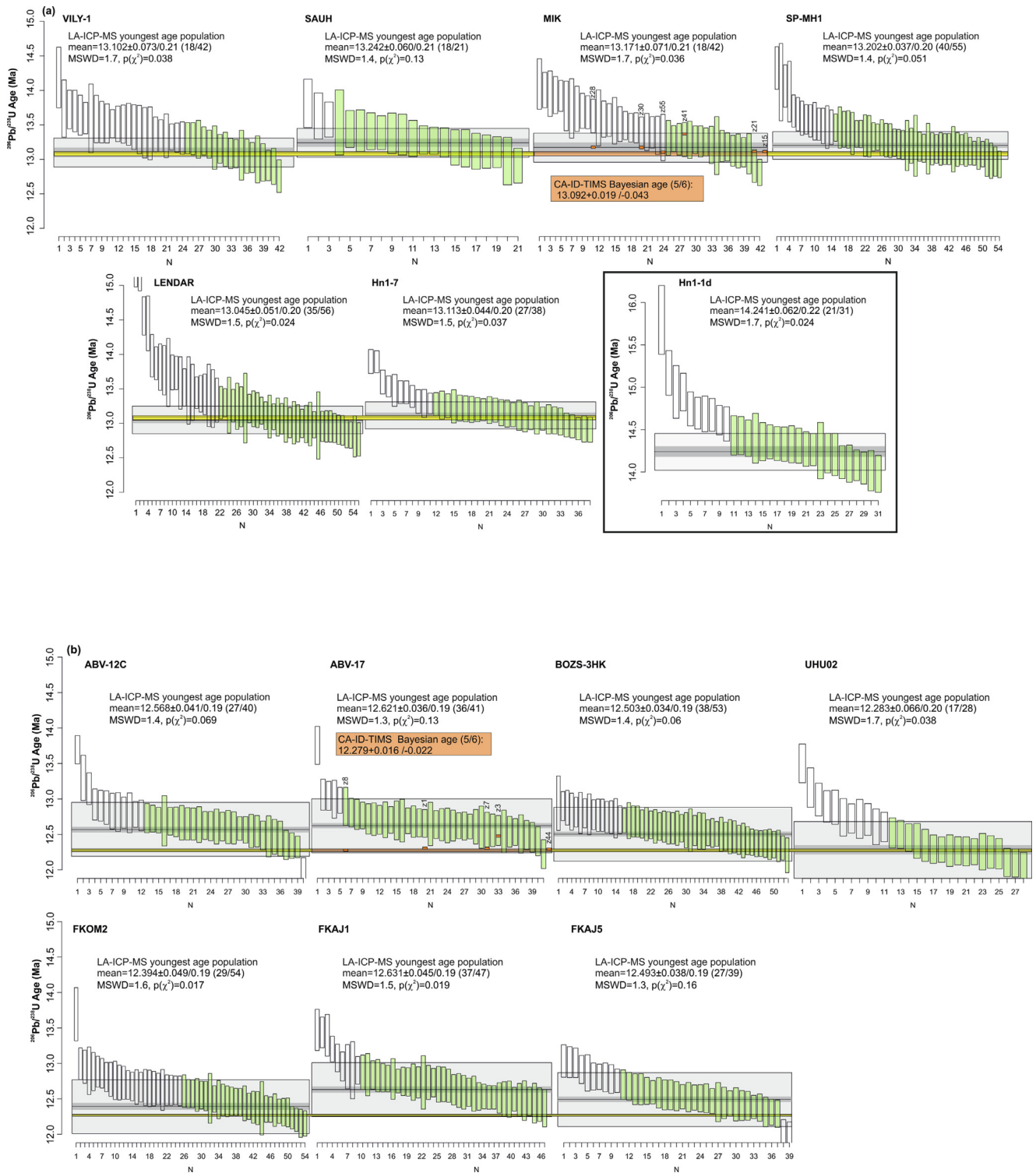


Fig. 3. $^{206}\text{Pb}/^{238}\text{U}$ zircon dates (in Ma) of the studied samples analysed by LA-ICP-MS and CA-ID-TIMS: (a) Samples belong to the Sátoraljaújhely (SAU) Unit and the sample Hn1-1d (inset); (b) Samples belong to the Hegyköz Unit; C. Samples belong to the Szerencs Unit; D. Samples belong to the Vizsoly Unit. LA-ICP-MS eruption ages are given as the weighted means of the youngest data (green bars) populations with internal 2 s uncertainties (dark grey)/propagated external 2 s uncertainties (light grey). Numbers in brackets after the ages correspond to the number of dates included in the youngest population out of the measured Miocene concordant dates. CA-ID-TIMS dates are indicated by orange bars at their corresponding LA-ICP-MS dates and/or by crystal identification numbers. Preferred CA-ID-TIMS eruption ages are depicted with an orange line that is extended in yellow to the other samples of the unit. (For interpretation of the references to colour in this figure legend, the reader is referred to the web version of this article.)

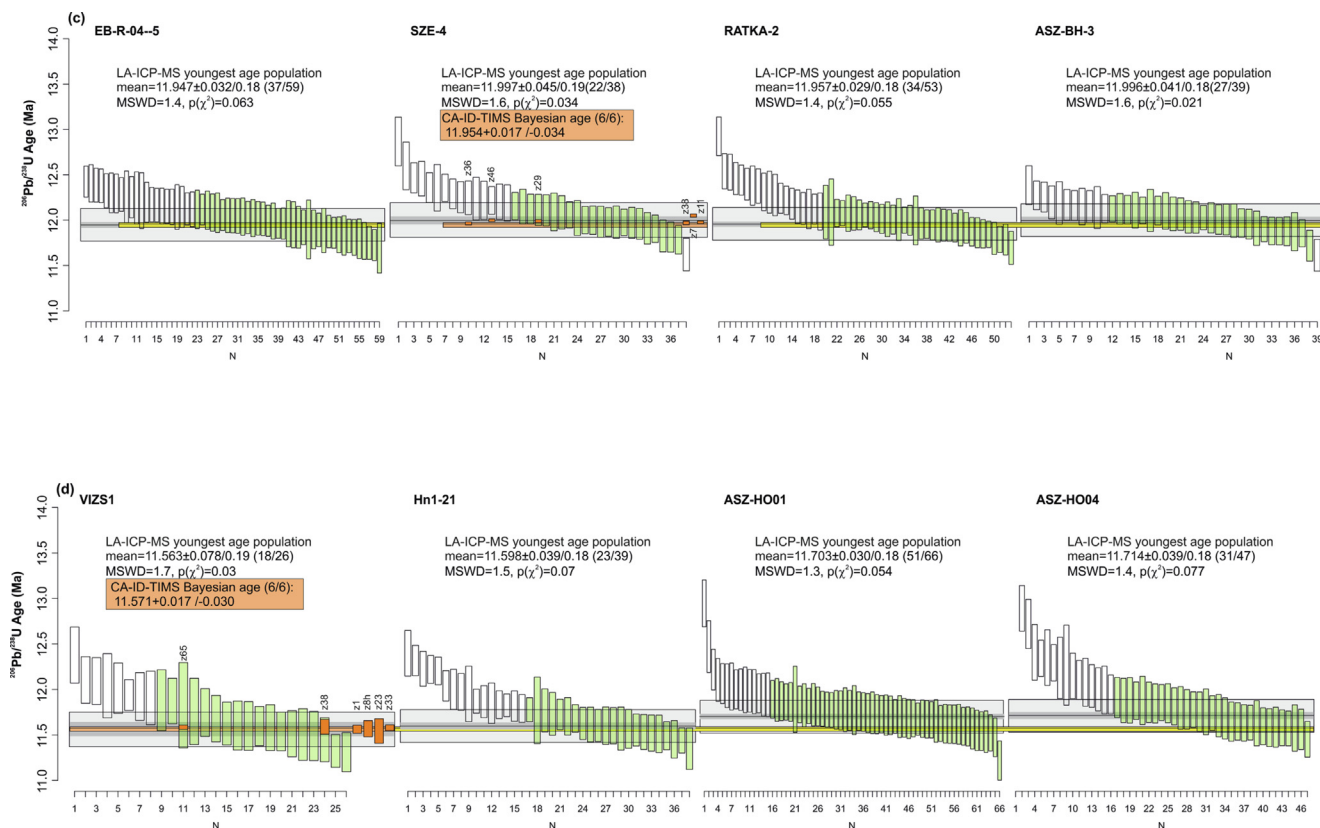


Fig. 3 (continued)

5.4. Volcanic glass and bulk rock chemical composition

We analysed bulk rock compositions from all units, including nearly all samples used for zircon geochronology as well as additional samples that were previously regarded as part of the units (data in [Supplementary Data, Table S3](#)). Chemical composition of volcanic glass shards of nine fresh, unaltered samples was also determined: four samples from the Hegyköz Unit, one from the Szerencs Unit, three from the Vizsoly Unit and the LENDAR sample (data in [Supplementary Data, Table S3](#)).

All studied samples are rhyolitic in composition with glasses having 73.1–78.1 wt% SiO₂, (normalized to 100 % anhydrous composition; original totals are mostly between 94 and 98 wt%), 11.1–15.8 wt% Al₂O₃ and total alkali content of 6.5–9.3 wt%, while bulk rocks have 73.0–77.9 wt%, 12.8–14.7 wt%, 8.0–10.6 wt% values, respectively. Both bulk rocks and glasses show typical enrichments in Cs, Rb, Th, Pb and K, while variable negative anomalies can be identified in case of Ba, Nb, Sr, P, Zr, Eu and Ti ([Fig. 7](#)). Rare earth element diagrams show enriched LREE, relatively flat HREE and strong, but variable negative Eu-anomaly that correspond to (La/Yb)_N ratios of 4.8–10.5 and Eu/Eu* values of 0.08–0.48 for bulk rocks and 1.33–10.14 and 0.008–0.49 for glasses, respectively. The main features of the trace element patterns of the glasses and bulk rocks are similar ([Supplementary Data, Sheet 3](#)) with minor differences towards more evolved compositions in the glasses. The SAU samples did not contain fresh glass; however, their bulk rock trace element data have notable similarities with the LENDAR bulk rock sample ([Supplementary Data, Sheet 3](#)). Samples related to the Hegyköz Unit show strikingly similar glass chemical and bulk rock compositions ([Supplementary Data, Sheet 3](#)), suggesting their common origin.

The SiO₂ shows no systematic variation with trace elements of glasses. The lowest SiO₂ content (73–75 wt%) is shown by the

ASZ-HO04, while all the other samples have similar ranges between ~75–78 wt%. On the contrary of bulk rock data ([Supplementary Data, Sheet 3](#)), the ASZ-HO01 glasses yield extremely high Rb and high K₂O contents that are not consistent with magmatic fractionation processes, therefore these data were not used in the interpretations ([Fig. 7](#)). ASZ-HO01 and ASZ-HO04 show differences in other elements, too and are both distinct from the VIZS-1 sample ([Fig. 7](#)). The remaining samples show a positive correlation between Rb, B, U and Nb and a negative correlation between these elements and Ba, Sr, Eu. The eruption units can be clearly distinguished based on trace element data, such as Ba, Sr, U, Eu/Eu*, La/Yb ([Fig. 7](#)). Only the LENDAR glasses have significant within-sample heterogeneity. A few of them partially overlap with the Hegyköz glasses, while the other glasses have a more evolved composition with low Ba and Sr contents. It is noteworthy that glass shards with a composition close to that of the Hegyköz sample, have similar trace element patterns to the bulk rock ([Supplementary Data, Sheet 3](#)). Glass shards from Szerencs Unit show a bimodal compositional signature, although both groups differ from those of the other eruptive units, particularly in the very low Ba and Sr contents.

6. Discussion

6.1. Identification of silicic explosive eruption units

6.1.1. Eruption chronology of large silicic eruption episodes

Previous K-Ar dating ([Pécskay et al., 1986, 1987, 2006; Pécskay and Molnár, 2002; Zelenka et al., 2012](#)) suggested long-lasting silicic explosive volcanism in the Tokaj Mts. from 15.2 Ma to 11.2 Ma. Between the major eruptions, andesitic to rhyolitic magmas built up lava domes and composite volcanoes presumably in or associ-

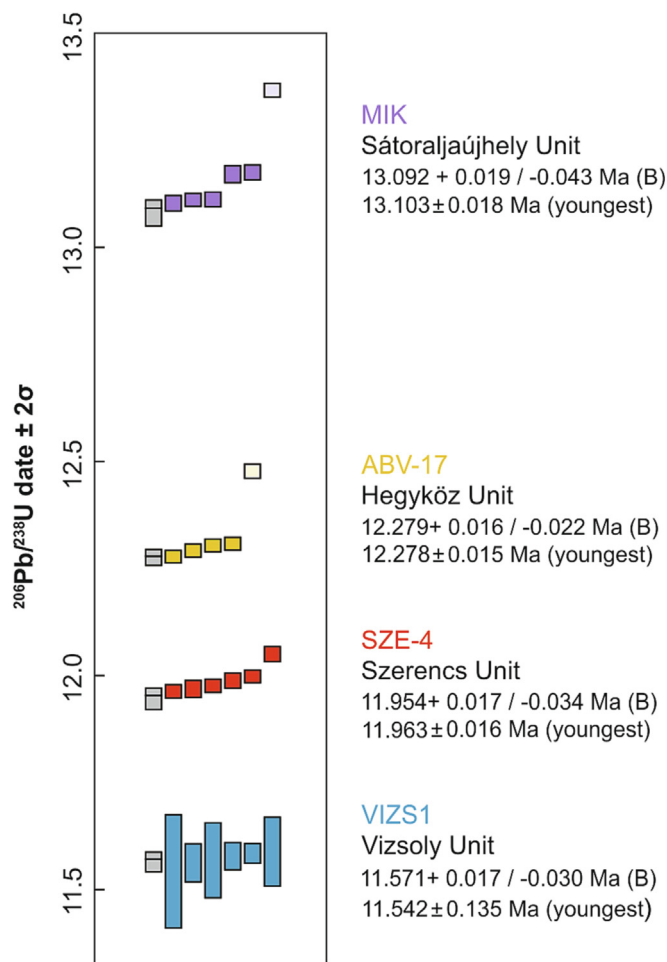


Fig. 4. CA-ID-TIMS geochronology: Age-ranked individual zircon $^{206}\text{Pb}/^{238}\text{U}$ dates and Bayesian eruption age estimates (B, grey bars) following Keller et al. (2018). Vertical bar heights represent 2sigma analytical and calculated uncertainties.

ated with the caldera structures formed during the explosive eruption events fed by silicic magmas. Our new zircon U-Pb age data refine this timespan, pointing to shorter and younger volcanic activity occurring in this area. The youngest population ages obtained from in-situ LA-ICP-MS dates yielded four age groups, which provide a first-order estimate of the eruption ages. Bulk single-grain ID-TIMS zircon dates of the representative samples from these units refine the eruption ages derived from the in-situ dating.

The new zircon U-Pb dating indicates four distinct periods of major explosive eruptions of silicic magmas in the Tokaj Mts., two of them presumably associated with caldera formations. The oldest eruption products of this area belong to the SAU, where

ID-TIMS yields an age of $13.092 \pm 0.019/-0.043$ Ma; Fig. 4 and Table 2), while the in-situ ages are between 13.1 ± 0.2 Ma and 13.24 ± 0.2 (Fig. 3A and Table 1). Notably, these ages are much younger than the existing K-Ar ages (around 15 Ma; Pécskay and Molnár, 2002; Pécskay et al., 2006). This can be explained by the variously altered nature of the host rocks and their main mineral phases, while zircon is resistant and preserved the primary features. The silicic pyroclastic rocks of the SAU are considered to represent the oldest volcanic products in this area, since they deposited either directly on pre-Cenozoic basement rocks or within the (late) Badenian marine sedimentary deposits. We obtained an indistinguishable zircon U-Pb age for the Hn1-7 drill core sample (13.1 ± 0.2 Ma; Table 2), which is derived from a 120 m thick massive ignimbrite bed in the borehole Hn-1 (Fig. 2), at the western margin of the TM (Fig. 1).

In addition, the same zircon U-Pb age (13.1 ± 0.2 Ma) was obtained also for the pyroclastic flow deposit at Lénárddaróc (Kakarcsó Hill, 5.22.LD4 = LENDAR sample) ~ 100 km westward. Thus, this eruption product is not part of the 14.4 Ma Harsány eruption as previously thought based on the bulk rock composition (Lukács et al., 2022). In the surrounding area, no volcanic rocks of similar age have been found; the only 13.1 Ma pyroclastic rocks are those of the SAU, which has similar geochemical composition as the older Harsány ignimbrite. If the LENDAR sample belongs to the SAU with an eruptive centre in the eastern TM, a large caldera-forming eruption would likely be required to produce a several tens of kilometre runout of the pyroclastic density currents. Far-running (>100 km) pyroclastic flows related to large, caldera-forming eruption were documented by Roche et al. (2022) for the Peach Spring Tuff (USA) and Takarada and Hoshizumi (2020) for the Aso-7 (Japan) eruptions as well as by Brlek et al. (2023) for the 18.1 and 17.3 Bükkalja eruptions. Such a long runout can be related to large, caldera-forming eruptions with high mass flow rates and channelization by palaeovalleys. Correlation between the thick SAU and the distal Lénárddaróc pyroclastic flow beds tentatively suggests that this eruption could have been enormous, yielding potentially several hundreds of cubic kilometre volcanic material. The age of the SAU eruption (13.1 Ma) defines the onset of the volcanism of the Tokaj Mts., which started later compared to the volcanic activity westward, in the Börzsöny–Visegrád Mts., Central Slovakian Volcanic Field, Mátra (ca. 15–16 Ma; Pécskay et al., 2006, Chersnysev et al., 2013) and also well after the large explosive volcanic events at Bükkalja (18.1–14.4 Ma; Lukács et al., 2018).

Some 800 ky later, another significant explosive eruption series occurred, resulting in the deposition of the Hegyköz Unit. Several pyroclastic samples thought to belong to this unit were dated, with in-situ ages ranging between 12.3 ± 0.2 Ma and 12.6 ± 0.2 (Table 1; Fig. 3B). High-precision ID-TIMS zircon analyses of the sample ABV-17 from this unit yielded an age estimate of $12.279 \pm 0.016/-0.022$ Ma (Fig. 4 and Table 2), which is resolvably younger than the one obtained by in-situ dating of the same sample (12.6 ± 0.2 Ma; Fig. 3B). Interestingly, comparing individual in-situ dates of

Table 2

Zircon-based eruption age estimates using CA-ID-TIMS U-Pb dates. Internal (int) uncertainty includes analytical uncertainty only, external (ext) uncertainty includes propagated analytical, tracer calibration and decay constant uncertainties (Jaffey et al., 1971). *Bayesian eruption age estimates following Keller et al. (2018) using a truncated normal prior distribution. n = number of analyses used from all analyses, σ = sigma.

Sample	youngest zircon		Bayesian age*				weighted mean		
	Age (Ma)	2σ int/ext (Ma)	n	Age (Ma)	95 % Confidence Interval		n	Age (Ma)	2σ int/ext (Ma)
					- int/ext (Ma)	+ int/ext (Ma)			
VIZS-1	11.542	0.135/0.135	6/6	11.571	0.030/0.032	0.017/0.021	6/6	11.579	0.016/0.021
SZE-4	11.963	0.016/0.021	6/6	11.954	0.034/0.036	0.017/0.022	4/6	11.974	0.008/0.016
ABV-17	12.278	0.015/0.020	4/5	12.279	0.022/0.025	0.016/0.021			
MIK	13.103	0.018/0.024	5/6	13.092	0.043/0.044	0.019/0.025	3/6	13.109	0.010/0.018

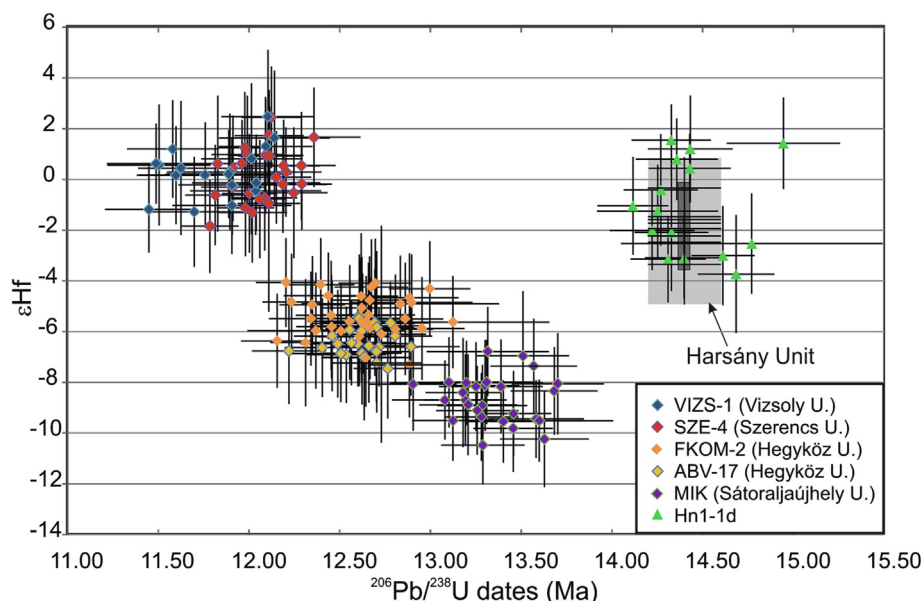


Fig. 5. Epsilon Hf (ϵ Hf) values of representative samples from the four units of the TM silicic explosive volcanic rocks and the Hn1-1d drill core sample are plotted with the closest/overlapping U-Pb spot dates (outliers and spots with discordant dates are not involved). The zircon ϵ Hf value range of the Harsány ignimbrite (Lukács et al. 2018) is shown for comparison.

the selected grains with their bulk ID-TIMS dates, there are two grains (z1 and z8, Fig. 3B) which differ significantly and give bulk-grain dates younger than the corresponding spot dates by ~ 300 (z1) and ~ 600 ky (z8). However, there is no systematic spot position and no recognizable CL texture that would explain this difference (Supplementary Data, Sheet 2). We ruled out analytical bias causing the discrepancy by repeated in-situ analysis of mounted grains from the sample and concluded that the difference is geological. Therefore, we suggest that both sets of dates are accurate and that the age difference may be related to volumetrically minor older zircon domains, not clearly recognizable on CL images, which were included in the sampling volume of in-situ analyses but did not shift bulk-crystal dates toward significantly older ages, either because of their minor volume or due to effective dissolution during chemical abrasion. We propose that the 300 ky range of eruption ages obtained for the Hegyköz Unit samples by in-situ dating may be the result of slightly older (antecrystic) grains or similarly unidentified older domains, which may indicate that they belong to a common eruption event or closely spaced events within a maximum of 300 ky around 12.3 Ma. This is supported by the observations in drill core (Fig. 2) where the pyroclastic rocks of the Hegyköz Unit are separated by rhyolitic lava intercalations. These volcanic products occur exclusively in the northern part of the Tokaj Mts. and presumably had a source in that area. In the Hn-1 borehole, the redeposited facies of this eruption unit can be identified as a 28 m thick volcanoclastic deposit (HN1-17; Fig. 2; Supplementary Data, Table S1). The cumulative 100–150 m thickness of the Hegyköz ignimbrites and the occurrence of the individual lithoclast-rich flow channels in the upper subunit suggest relatively less voluminous eruptions compared to SAU. They were also presumably closely related to lava dome volcanism (Szepesi et al., 2019).

The third explosive eruption period is connected to the Szerencs caldera identified beneath the present surface by geophysical surveys at the southwestern margin of the TM (Hegedűs et al., 2002; Zelenka et al., 2012). Pécskay and Molnár (2002) suggested, based on K-Ar results, that the caldera-forming eruption occurred between 12.2 Ma and 11.3 Ma. This age is confirmed by our zircon

dating, with a more accurate result of $11.954 \pm 0.017/-0.034$ Ma by ID-TIMS and 12.0 ± 0.2 Ma by LA-ICP-MS (Fig. 3C, 4, Table 1, 2). This eruption started with pyroclastic falls in a marine environment followed by massive ignimbrite units reaching several hundred metres in thickness at Szerencs. Remarkably, the pyroclastic deposits derived from the Szerencs eruption were not recorded in the Hn-1 borehole, instead the volcanic eruption could have affected mostly the areas southward.

The fourth silicic explosive eruption episode (Vizsoly Unit) is identified at the western margin of the volcanic area. The in-situ zircon U-Pb eruption ages are between 11.6 ± 0.2 and 11.7 ± 0.2 Ma, while the ID-TIMS results yield an eruption age estimate of $11.571 \pm 0.017/-0.030$ Ma (Fig. 3D, 4; Table 1, 2). This is a massive unwelded ignimbrite, up to 100 m in thickness, with unknown source which was likely close to Vizsoly. In the Hn-1 borehole, a similar age for the sample of the uppermost, 10 m thick pyroclastic bed was obtained (Hn1-21; 11.6 ± 0.2 Ma; Fig. 2; Table 1). Noteworthy, further smaller eruptions, although from different magmas occurred also right coevally with the Vizsoly eruptions as shown by the ASZ-HO01 and ASZ-HO04 samples.

In summary, on the grounds of zircon U-Pb ages, we propose that four major rhyolitic explosive eruption phases occurred in the Tokaj Mts. between 13.1 and 11.6 Ma. They might involve single events, or several eruptions closely spaced in time, within a maximum of a few hundred ka. Two of them (SAU and Szerencs U.) appear to have been large and associated with caldera formation. The major explosive eruption phases were separated by several hundred thousand years when rhyolitic lava domes and andesitic volcanic edifices were developed. The new zircon ages suggest a shorter timespan (1.5–2 My) of the volcanism in Tokaj Mts. and importantly, they imply that it started later (13.1 Ma instead of 15.2 Ma) than the previous K-Ar ages (Pécskay et al., 2006) showed. Additionally, the lowermost pyroclastic unit in the Hn-1 borehole gave a significantly older age (14.2 ± 0.2 Ma), which chronostratigraphically resembles the 14.4 Ma Harsány Unit, the youngest silicic explosive eruption unit of the Bükkalja volcanic field (Lukács et al., 2015, 2018). This early Badenian age is in agreement with the paleontological founding just below the

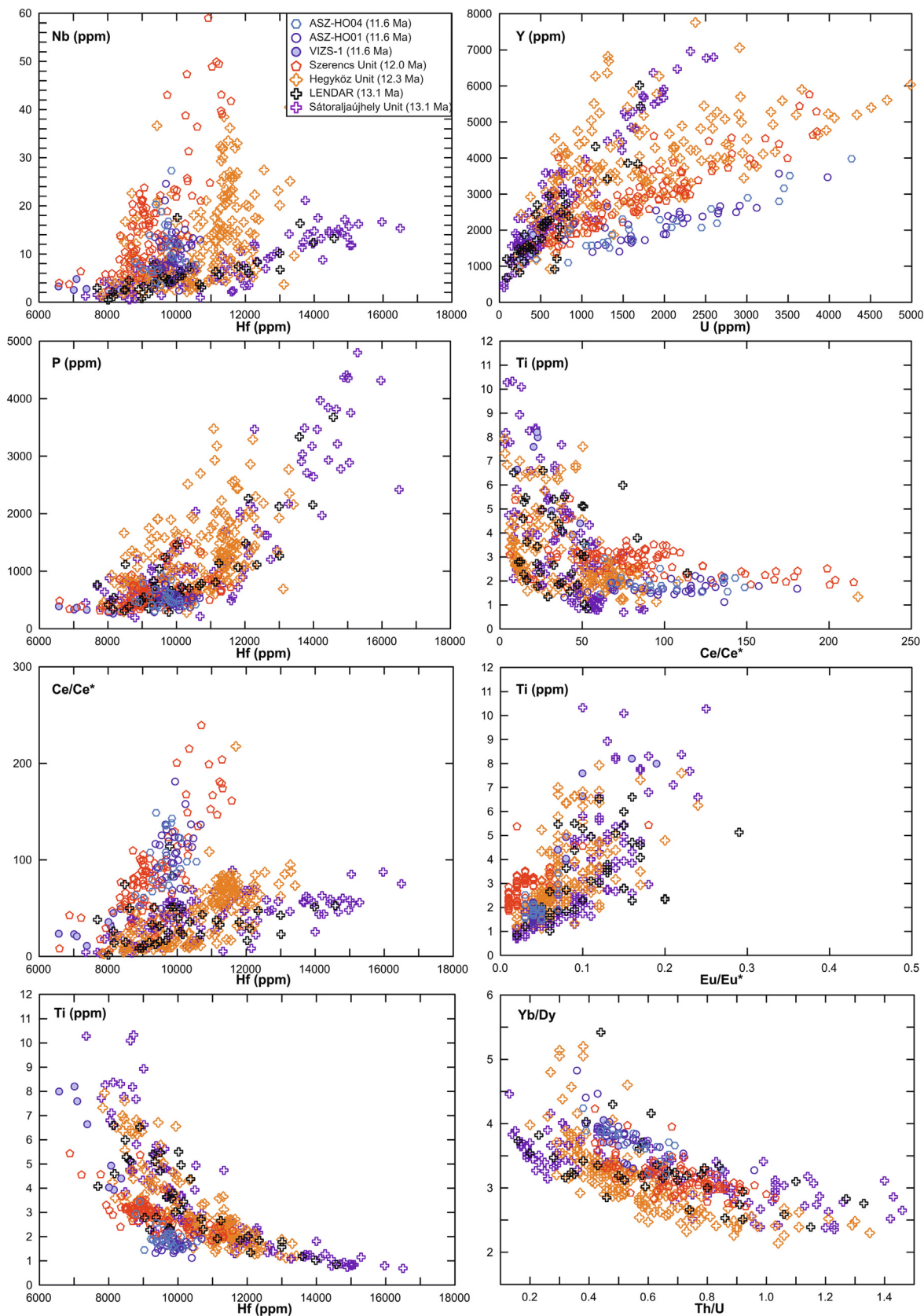


Fig. 6. Trace element and trace element ratio (Th/U, Yb/Dy, Eu/Eu*, Ce/Ce*) variations in the zircon of various explosive eruption units of the TM.

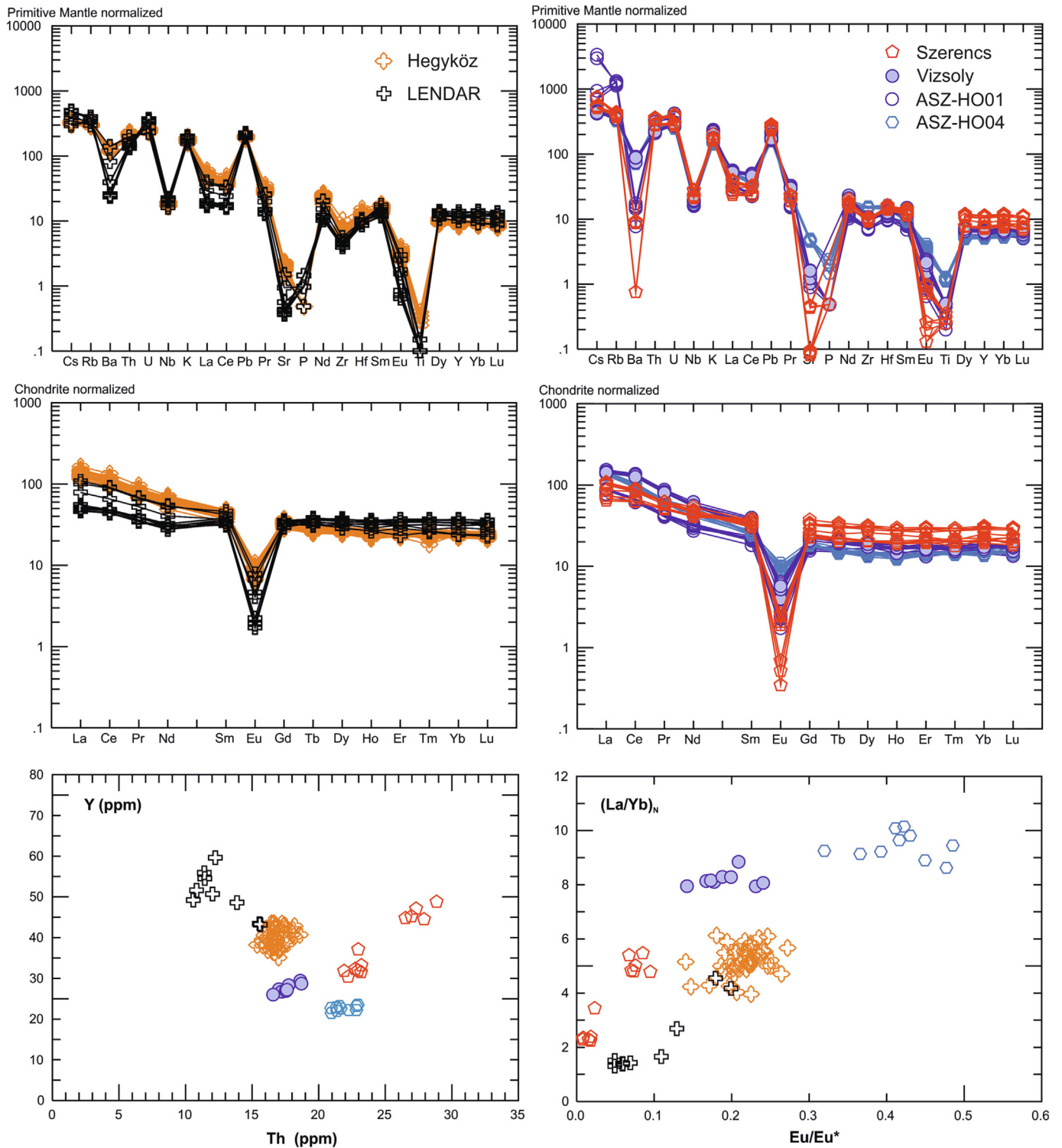


Fig. 7. Trace element characteristics of glass shards from the TM explosive eruption units (note that no fresh glass was found in the SAU, however, the fresh LENDAR glasses from a distal pyroclastic deposit can represent this eruption unit). Trace elements and trace element ratios can be effectively used to distinguish the samples from different units. Note also the compositional bimodality of the Szerencs Unit. Primitive mantle and chondrite composition values are from Sun and McDonough (1989).

pyroclastics that shows nanofossils indicating NN5 biozone (14.9–13.5 Ma; Bodor and Fodor, 2013). This is confirmed also by their overlapping ϵ Hf isotope data (Fig. 5; Supplementary Data, Sheet 3). This 4-meter-thick horizon (with relatively small pumices) suggests distal facies and could have originated from the same source as the Harsány Unit. Therefore, we propose that this pyroclastic bed is not a product of the Tokaj Mts. volcanism.

6.1.2. Eruption product correlation by combined zircon and glass trace element compositions

Zircon fingerprinting, i.e. a combination of in-situ U-Pb ages and chemistry (trace element and/or Hf isotopic composition) is a powerful tool to recognize scattered volcanic products and correlate them to a given eruption episode (Lukács et al., 2021). In the case of the Early- to Mid-Miocene large silicic volcanism of Bükkalja,

this technique was successfully used to link distal deposits to proximal ones even when the host pyroclastic rocks were thoroughly altered. More recently, this methodology was applied to volcanic occurrences around the Pannonian Basin (in Croatia, Austria and Romania; Bercea et al., 2023; Brlek et al., 2023; Šegvić et al., 2023) and this enabled to correlate these deposits to the main eruption units identified by Lukács et al. (2018) in Bükkalja. Here, we used this technique in combination with the glass composition of unaltered samples to check whether the erupted magmas in Tokaj Mts. possess unique compositional characteristics, which can be used for correlation purposes. Multivariate mathematical techniques (principal component analysis, linear multivariate discriminant analysis) were applied taking into account as many variables as possible and useful. Pre-defined groups were made based on the zircon U-Pb ages and we checked whether they are also distinct based on their zircon trace element composition, i.e. the erupted magma had a unique geochemical fingerprint. Note that the Vizsoly Unit as represented by the VIZS-1 sample was treated as a distinct group even though the ASZ-HO01 and ASZ-HO04 samples gave the same zircon U-Pb ages. Zircon trace element data proved that they cannot be derived from eruption of the same magma. To avoid spurious results, we omitted all variables which showed high correlation with others and involved also trace element ratios that appeared to be distinctive based on bivariate plots (Fig. 6). Thus, the following trace elements and trace element ratios were involved in the multivariate calculations: Hf, U, Y, Nb, Nd, P

and Eu/Eu*, Th/U, Yb/Dy. We applied a logarithmic transformation of these variables. The weights on the linear discriminant functions indicate how these variables contribute to discriminate the defined groups in the multivariate space (Table 3).

Among the applied variables, U, Hf, Y, the Yb/Dy ratio and the Eu/Eu* are the most significant to discriminate the four eruption units as well as the ASZ-HO samples (Fig. 8). The five pre-defined zircon groups can be readily distinguished in the space of the 1st and 2nd linear discriminant functions. The ASZ-HO samples indeed differ from the zircon population of the Vizsoly Unit. The two older eruption units can be distinguished primarily based on their U and Y content, whereas the Szerencs Unit is characterized by very low Eu/Eu* values. The Vizsoly Unit has a transitional, but well-distinguished position between the SAU and Szerencs Units. Plotting the LENDAR zircon data on the LDA1 vs. LDA2 discriminant diagram, a perfect overlap is found with the SAU samples, clearly proving that this distal eruption product derived from the SAU eruption (Fig. 8).

Zircon trace element characteristics reflect the compositional feature of the long-standing crystal-mush reservoir, whereas the glass trace element data indicate the nature of the erupted melt-dominated fractions of these reservoirs. Nevertheless, the similar compositional characters, particularly in the U, Y and Eu/Eu* of the zircon (Fig. 6) and glass (Fig. 7) suggest that the highly differentiated melt composition controlled the zircon trace element content. Glass trace element values are usually effectively used to

Table 3

Weights of the selected variables on the linear discriminant functions in the multivariate linear discriminant analysis result [i.e., $LDAx = \sum_{i=1}^n \beta_{LDAxi} \cdot (y_i - \alpha_i)$, where x , y_i , α_i and β_i are the discriminant components (i.e., 1, 2, or 3), the features (i.e., logP, logY, etc.), scaling factors (i.e., average values), and the LDA coefficients, respectively].

Coefficients for linear discriminant functions				
	β_{LDA1}	β_{LDA2}	β_{LDA3}	α
log P	1.6102	-0.3876	0.8825	6.7410
log Y	1.9225	5.0637	-4.1712	7.9394
log Nb	1.0916	1.6112	1.3136	2.2118
log Nd	-1.0253	-1.8585	2.7581	0.7854
log Hf	12.6032	-1.5181	-0.5672	9.2245
log U	-3.1195	-5.0747	0.5273	7.0484
log Eu/Eu*	3.1797	-1.4978	-0.6469	-2.9374
log Th/U	0.9714	2.7002	-3.1530	-0.5631
log Yb/Dy	-4.4704	1.5754	-4.6738	1.1661

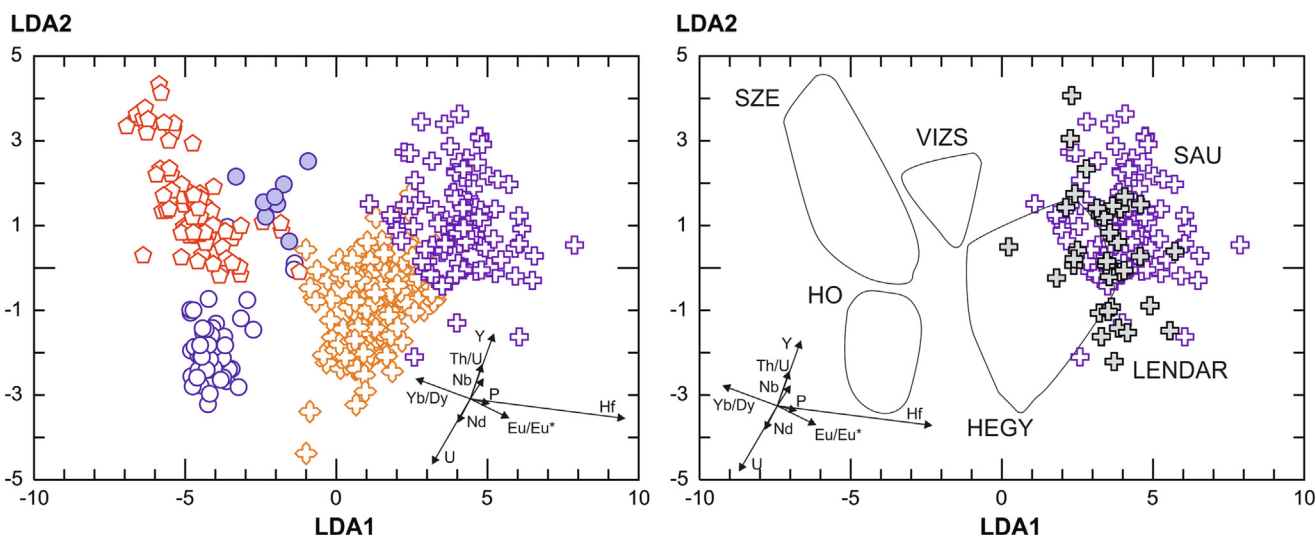


Fig. 8. (a) The multivariate linear discriminant analysis distinguishes the eruptive units based on zircon trace element compositions. The relative weights of the used variables are illustrated by vector arrows (variables are in log unit). (b) The distal Lénárddaróc pyroclastic beds show remarkable compositional overlap with the SAU; the trace element similarities along with the same zircon U-Pb age suggest that they derived from the same eruption. Eruptive units: SZE = Szerencs; VIZS = Vizsoly; HO = ASZ-HO samples, Hidegoldal (Abaújszántó); HEGY = Hegyköz; SAU = Sátoraljaújhely; LENDAR = Lénárddaróc. Symbols are explained in Fig. 6.

distinguish eruption units, but only if no subsequent alteration affected the original features. In the latter case, zircon is the only witness of the erupted magma (e.g., SAU) likely reflecting the melt composition. Since zircon trace element composition as well as U-Pb age suggest that the LENDAR deposit derived from the SAU eruption, the LENDAR glass is used to represent the erupted melt component of SAU. In-situ glass trace element data confirm that the four silicic explosive eruptions were fed by geochemically distinct magmas (Fig. 7). Each eruption unit is characterized by coherent trace element content, except for the Szerencs samples, where a compositional bimodality is recognized (both in glass and zircon trace element compositions).

6.2. Petrogenesis of silicic magmas

6.2.1. Origin of the erupted crystal-poor magma

The Tokaj Mts. volcanic area is a unique example of the andesitic to dacitic volcanism in the Pannonian Basin with a strong contribution of rhyolitic magmas. In other Mid-Miocene to Quaternary volcanic complexes of this region, rhyolites are scarce and intermediate magmas dominate (Lexa et al., 2010). Based on a detailed fieldwork and zircon geochronological study, four main explosive eruption periods involving silicic magmas were distinguished. Although most of the volcanic products are variably altered (zeolitization, silicification), fresh samples were also found. They are all crystal-poor (crystal content is up to 12 vol%) high-silica ($\text{SiO}_2 > 70\text{-wt}\%$) rhyolites with variable amounts of quartz and feldspars, minor biotite and occasionally pyroxenes. Such magmas can represent residual melts of extreme fractional crystallization at shallow depths (Blundy and Cashman, 2001). Modelling results based on R-MELTS (Gualda et al., 2012) confirm the low-pressure crystallization providing 120–150 MPa values, which are consistent also with the haplogranitic ab-qz-or ternary phase diagram results (Tuttle and Bowen, 1958, updated by Johannes and Holtz, 1996; Blundy and Cashman, 2001), where the composition of the Vizsoly glasses (the only one where $\text{ASI} < 1.1$) fall between the 100–200 MPa minimum points (Supplementary Data, Sheet 3).

The evolution of the evolved silicic melt before the large explosive eruptions in Tokaj is modelled on the basis of the relative concentrations of Sr, Ba and Rb (Halliday et al., 1991; Anderson et al., 2000; Bachmann and Bergantz, 2004). Strontium shows low values, less than 50 ppm in most of the glasses (the only exception being the ASZ-HO04 samples, where Sr is between 90 and 100 ppm) and extreme low values (<5 ppm) in the Szerencs glass

populations (Fig. 9). Such extreme low Sr content in rhyolites is rare (Halliday et al., 1991), examples are the Bishop Tuff (Chamberlain et al., 2014) and Glass Mt. in the Long Valley caldera (Davies and Halliday, 1998) and the Huckleberry Ridge Tuff (HRT) of the Yellowstone caldera (Swallow et al., 2019). Other large rhyolitic systems, such as Oruanui, Taupo (Allan et al., 2017), Aso-4 (Keller et al., 2021) and Toba, Indonesia (Westgate et al., 2013; Pearce et al., 2020) along with the data from the Bükkalja volcanic field, Pannonian Basin (Harangi et al., 2005; Karátson et al., 2022) have typically higher glass Sr content (>30 ppm; Fig. 9), i.e., they have less evolved character. Rubidium concentration in the Tokaj glasses is within a relatively narrow range of 170 ppm to 270 ppm, while Ba has wider compositional variation from a few ppm up to 900 ppm. The Rb shows a negative correlation with the Sr values, whereas there is a positive correlation between Ba and Sr (Fig. 9). Notably, the glass composition is relatively homogeneous within-samples, except for the distal LENDAR ignimbrite, where variable composition is found and the Szerencs Unit rhyolites, where a bimodality is recognized. The coherent glass compositional features suggest that the eruptions occurred from well-homogenized, melt-dominated bodies. The Szerencs eruption could involve separated melt lenses with slightly different rhyolitic compositions (Fig. 9) as shown also for the Younger Toba tuff (Westgate et al., 2013; Pearce et al., 2020), the Whakamaru eruption (Saunders et al., 2010) and the Huckleberry Ridge Tuff, Yellowstone (Swallow et al., 2019).

The variation in Sr-Ba-Rb concentrations suggests that Sr and Ba were compatible during the latest magma evolution, while Rb remained incompatible. The extremely low Sr (<10 ppm) in the Szerencs and in some of the LENDAR glasses requires high bulk D^{Sr} values (e.g., up to 50 in case of Glass Mt., Halliday et al., 1991) consistent with progressive feldspar crystallization. This is reflected also by the very low Eu/Eu^* values (<0.1) in both the glasses and zircon of these samples, implying that zircon crystallization occurred even well after the major feldspar fractionation from a highly evolved silicic melt. Trace element model calculations were performed using the logarithmic Ba/Rb and Sr/Rb ratios to estimate the relative proportions of plagioclase and sanidine during the latest crystallization (Fig. 10). We used the same partition coefficients as provided by Anderson et al. (2000) and initial melt compositions of Sr = 50 ppm, Rb = 150 ppm and Ba = 1050 ppm. The result reproduces well the Tokaj glass composition data, suggesting crystallization at different plagioclase/sanidine ratios, but similar parental magma composition, akin to that

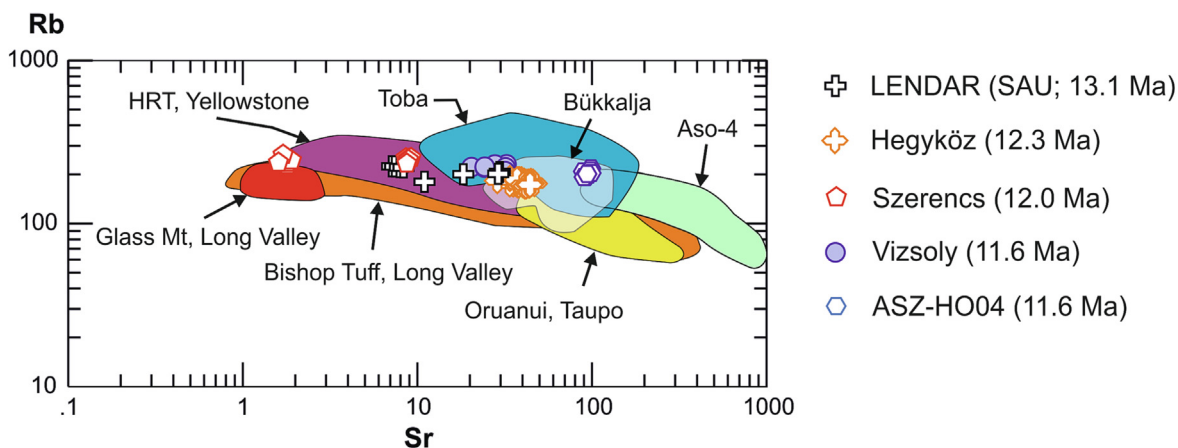


Fig. 9. Glass Sr vs. Rb distribution (both elements are in ppm) of the studied TM silicic explosive units compared with data of selected large silicic eruptions (Glass Mt: Davies and Halliday, 1998; Bishop Tuff: Chamberlain et al. 2014; Huckleberry Ridge Tuff, Yellowstone: Swallow et al., 2019; Oruanui, Taupo: Allan et al., 2017; Younger Toba Tuff: Westgate et al., 2013; Pearce et al., 2020; ASO-4: Keller et al., 2021; Bükkalja: Lukács et al., 2018). Note the strong Sr depletion in the Szerencs eruption unit and to a lesser extent, in the Lénárdaróc (LENDAR) glasses that represent the SAU eruption.

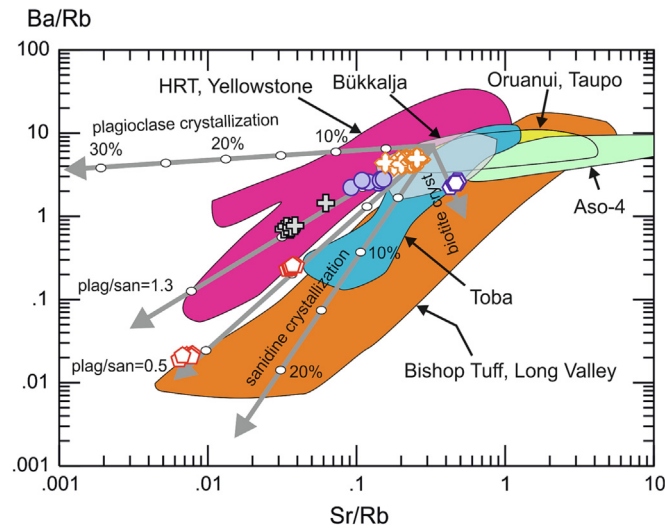


Fig. 10. Glass Sr/Rb vs. Ba/Rb plot to illustrate the crystal fractionation in the studied TM silicic explosive units (symbols as in Fig. 9). The rhyolitic magmas evolved by dominant feldspar crystallization with various amounts of sanidine and plagioclase similarly as the Huckleberry Ridge Tuff, Bishop Tuff and the Toba magmas, whereas in other large silicic eruptive products no significant sanidine crystallization occurred. The ASZ-H004 glasses appear to reflect biotite fractionation. Fractional crystallization vectors of plagioclase, sanidine and biotite were calculated using the distribution coefficients given by Anderson et al. (2000). The TM glasses can be modelled via crystallization of plagioclase/sanidine ratio of 1.3 (SAU) and 0.5 (Szerencs Unit) at about 10–15% quartz and minor biotite. Reference data of comparative rhyolitic systems as in Fig. 9.

shown by the Bükkalja rhyolites. The Szerencs silicic magma could have crystallized at a lower plagioclase/sanidine ratio (0.5) than the SAU–LENDAR and Vizsoly magmas (plag/san = 1.3) with about 10–15 % quartz and minor biotite. Melt lenses in the Szerencs magma reservoir could be cogenetic, separated at slightly different evolutionary stages from the same evolving magma. Biotite crystallization had a stronger control on the evolution of the ASZ-H004 magma. Such extremely evolved silicic magmas can represent interstitial melts in a high crystallinity (crystals are 60–80 vol%) shallow seated magma body (Bachmann and Bergantz, 2004; Hildreth, 2004). The low crystal content implies effective segregation from the crystal network and limited further crystallization prior to eruption. Since model calculation implies 20–30 % crystallization to reproduce the melt composition from an already rhyolitic parental melt and crystal content of the erupted magma is less than 10–15 %, these evolved melts could have largely originated within the crystal mush and melt extraction was presumably rapid. Remobilization and fast melt segregation characterized the Oruanui magma reservoir with an inference that this took place mostly within 200 years (Allan et al., 2017). Such magma storage re-establishment results in either a single large melt-dominant body, which can be inferred for most cases in the TM silicic magma reservoirs, whereas before the 12.0 Ma Szerencs eruption, distinct melt lenses could have been developed and contributed to the erupted magma body.

6.2.2. The nature and residence time of the silicic crystal mush body

The state and evolution of the silicic crystal mush can be constrained by in-situ zircon U–Pb dates, Hf isotopes and trace element composition data. Zircon from the four explosive units shows well-developed magmatic zonation in CL images with only rare clearly identifiable xenocrystic cores, which are mostly in samples from the SAU with xenocrystic core ages between 760 and 200 Ma (Supplementary Data, Sheet 2). Compared to other rhyolitic rocks in

this volcanic area, the relative rarity of old grains and xenocrystic domains in zircon from all other units is an important observation. Interestingly, Kohút et al. (2021) defined an age interval from 12.07 ± 0.37 to 11.44 ± 0.39 Ma based on ^{39}Ar – ^{40}Ar dating of the obsidians from the Zemplín-Tokaj (Brehov, Cejkov, and Viničky), north of our study area, that contain dominantly relict zircon with distinct age ranges, which were correlated with the ages of the nearby pre-Cenozoic bedrocks (Kohút et al., 2019). Only a few Miocene ages between 15 and 13 Ma were observed. In contrast, our studied samples contain few xenocrystic zircon domains. This difference between the rhyolite lava and pyroclastic rocks can point to the different magma evolution and to more time for zircon growth under zircon saturation state before the explosive eruptions. Furthermore, this suggests either hot, zircon-corrosive magmas or no/little crustal contamination during the magma evolution of the studied pyroclastic rocks. Zircon saturation temperature calculated from glass composition following the Watson and Harrison (1983) method is in the range 750–760 °C for the Szerencs and Vizsoly samples, whereas it is between 730 and 740 °C for the Hegyköz. An anomalously low temperature (around 700 °C) was obtained from the Lénárdaróc (LENDAR) glasses that could represent the oldest SAU. These temperature results, beside the crystal-poor nature of the rocks suggest that dissolution is unlikely (so xenocrysts are easier to preserve) and can be used as pre-eruptive magma temperature estimates (Miller et al., 2003). The relatively low temperature is consistent with the highly evolved melt compositions produced at haplogranitic minimum points as reflected by the glass trace element data.

The residence time (defined as the difference between the oldest zircon crystallization date and eruption ages, i.e., the interval when the melt was continuously present in the magma reservoir) of the silicic crystal mush bodies is inferred from the range of zircon dates. Considering the measured rim spot dates and taking into account ± 0.2 Ma uncertainties on these individual analyses, we can infer 1.1 My, 1.4 My, 0.8 My and 1.4 My zircon crystallization timescale for magmas of the SAU, Hegyköz, Szerencs and Vizsoly Units, respectively (Figs. 3, 4). These very long timescales presumably overestimate the real residence of the silicic magmas because of the presence of older antecrysts. A better constraint can be expected from the CA-ID-TIMS dates. They give 265 ky, 199 ky, 87 ky and 46 ky crystallization age ranges for these units and they can be regarded as minimum values. Thus, we can infer at least 46–265 kys, probably several 100's thousand years of magma residence time for the studied eruptive units. This is consistent with the reported up to 900 kyr magma residence times for silicic, caldera forming volcanic systems (e.g. 19–250 ky, Yellowstone, Gansecki et al., 1998; Bindeman et al., 2001; Vazquez and Reid, 2002; Stelten et al., 2015; Long Valley, 50–390ky, Davies and Halliday, 1998; Simon and Reid, 2005; 9–250 ky, Taupo Volcanic Zone, Brown and Fletcher, 1999; Charlier et al., 2005; Klemetti et al., 2011; <160 kyr, Toba, Vazquez and Reid, 2004; 180 ky, 80–900 ky, La Garita, Bachmann et al., 2007).

Trace element content and Hf isotope values of zircon provide information about the origin and evolution of the silicic magma bodies before the explosive eruptions in the Tokaj Mts. Epsilon Hf values show little variation within the eruption units, but a major change can be observed between the 12.3 Ma Hegyköz and the 12.0 Ma Szerencs Units (Fig. 5). The oldest, SAU zircon yields the most negative ϵHf values (-8.8 ± 0.5), while higher values are typical for the Hegyköz samples (-6.4 ± 0.6 to -5.3 ± 0.6). A distinctly higher and mostly overlapping values characterize the Szerencs ($\epsilon\text{Hf} = 0.1 \pm 0.6$) and Vizsoly ($\epsilon\text{Hf} = 0.2 \pm 0.7$) zircon populations. These isotope values have two important implications: (1) The zircon ϵHf values suggest that the crustal silicic magma reservoirs fed the large explosive volcanic eruptions in the Tokaj Mts. between 13.1 and 11.6 Ma contained distinct mag-

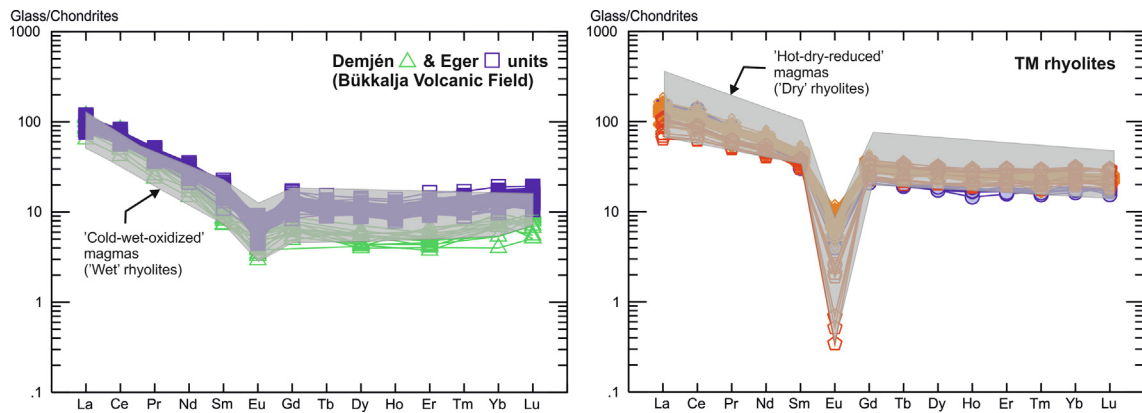


Fig. 11. Chondrite-normalized (Sun and McDonough, 1989) rare earth element patterns of the glass shards from the Bükkalja and Tokaj (TM) rhyolites compared to those of the so-called 'cold-wet-oxidized' and 'hot-dry-reduced' silicic magmas as defined by Bachmann and Bergantz (2008). Glasses of the Demjén and Eger units from the Bükkalja volcanic field show an overlap with the range of the 'cold-wet-oxidized' silicic magmas consistent with the occurrence of amphibole in these rocks. On the other hand, glasses from the TM rhyolites are distinct and have features akin to the REE-patterns of the 'hot-dry-reduced' silicic magmas. The less hydrous character of the TM rhyolites is reflected by the lack of amphibole and the sporadic occurrence of pyroxene.

mas with variable mantle/crustal components. The youngest 12.0 Ma Szerencs and the 11.6 Ma Vizsoly rhyolite magmas show remarkable isotopic similarity although they can be clearly distinguished by glass trace element characteristics. (2) The initial silicic magmas involved a significant crustal component, i.e., they could have been generated either by anatexis of lower crustal material or by notable crustal contamination of mantle-derived mafic magmas. With the lack of knowledge on the deeper part of the crustal material and its isotopic signature, the origin of these magmas cannot be constrained unambiguously. Nevertheless, within 1 My, a significant change in the silicic magma genesis occurred. The origin of the 12.0–11.6 Ma rhyolites (Szerencs and Vizsoly) can be explained by a larger contribution from mantle-derived magmas in comparison to the older units.

The zircon trace element signature of the Tokaj samples differs notably from that observed for the Bükkalja rhyolites (Supplementary Data, Sheet 3; Lukács et al., 2015, 2018, 2021). In general, they have pronounced negative Eu-anomaly (low Eu/Eu^* values: <0.2), high Y (up to 7000 ppm) and U (up to 5000 ppm) contents and relatively constant Yb/Dy ratio at low values (2–4). The very low Eu/Eu^* values of zircon are consistent with the notion stated above that strong feldspar crystallization occurred even in the crystal mush and only a minor further magma differentiation occurred after the melt extraction. The compositional features of zircon are consistent with the glass trace element characteristics and imply that the evolution of silicic magmas occurred at distinct conditions. Several units of the Bükkalja area, such as the Demjén and Eger ignimbrites show compositional features suggesting that amphibole played a role in the magma evolution, whereas glass compositions of the TM rhyolites reflect a liquid line of descent involving dominant feldspar crystallization in addition to pyroxenes (Fig. 10). For the TM rhyolites, the zircon oxybarometry (Loucks et al., 2020) results indicate redox conditions along the QFM buffer curve, i.e. a relatively reduced condition. Based on the distinct evolutionary paths, Christiansen (2005) and Christiansen and McCurry (2008) divided rhyolites occurring in the western Cordillera of the USA into two types, denoted as cold-wet-oxidized and warm-dry-reduced categories. Deering et al., (2008, 2010) also detected these two main rhyolite groups in the Taupo volcanic zone, where the relative proportions of amphibole, orthopyroxene and clinopyroxene phases governed the compositional evolution, i.e., under relatively wet (hydrous) and oxidized and relatively dry (less hydrous) and reduced states. Rare earth element patterns of glasses from the Bükkalja and Tokaj

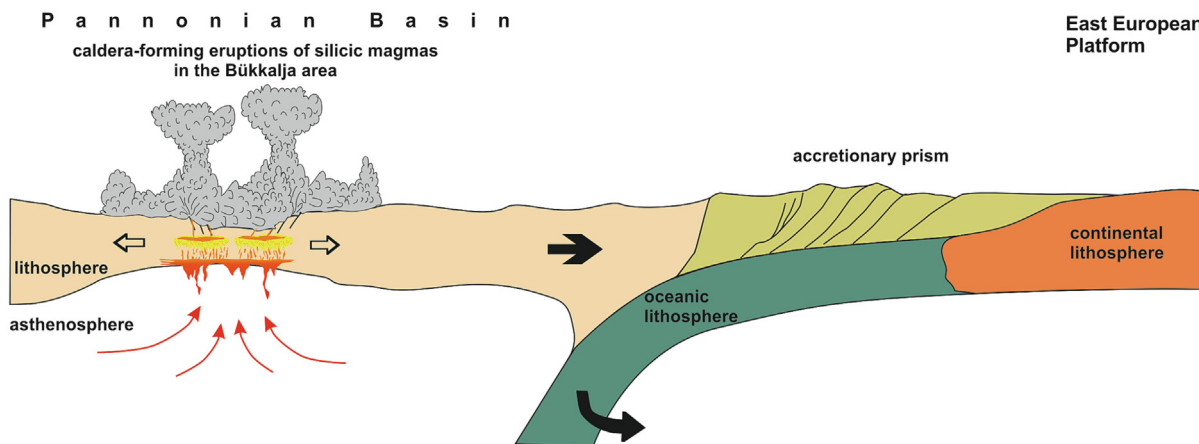
silicic volcanic rocks suggest that this compositional and evolutionary dichotomy can be observed also in the rhyolites of the Pannonian Basin (Fig. 11).

6.3. Geodynamic condition of the silicic volcanism

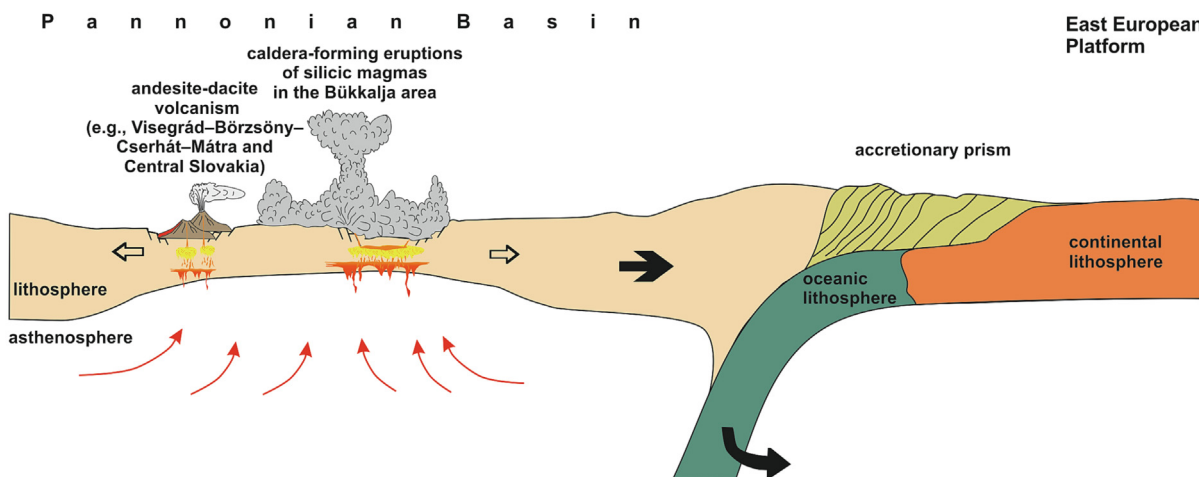
Large-volume explosive eruption of silicic magmas occurs mostly in subduction zone tectonic setting with thick continental crust, although extension contributes effectively to the formation of the crustal magma reservoir (Hildreth, 1981). However, extensive rhyolitic volcanism can be formed also at a tectonic setting with thinned crust and lithosphere behind a subduction zone (e.g., back arc rift of Taupo zone behind the oblique subduction along the southern segment of the Tonga-Kermadec arc, Hikurangi subduction margin; Cole, 1990; Houghton et al., 1995; Gravelly et al., 2016; Wilson and Rowland, 2016). There are also examples of intraplate continental settings, presumably hot-spots with mantle plume (e.g., Snake River Plain rhyolites ending with Yellowstone, Christiansen, 1984; Branney et al., 2008; Huang et al., 2015; Camp and Wells, 2021). The Pannonian Basin was formed by large-scale continental lithospheric extension developed progressively from southwest to northeast during a period between 22 Ma and 9 Ma (Fig. 12; Horváth et al., 2006, 2015; Balázs et al., 2016). The driving force of the extension was thought to be the subduction roll-back along the northeastern-eastern Carpathians (Fig. 12; Csontos et al., 1992; Nemčok et al., 1998; Maženco and Bertotti, 2000; Horváth et al., 2006), although gravitational potential energy derived from the Alpine orogeny was also invoked in association with lateral extrusion of the ALCAPA microplate from the compressive Alpine regime (Ratschbacher et al., 1991a, 1991b; Bada and Horváth, 2001; Ustaszewski et al., 2008). On the other hand, new numerical models emphasise the role of localized mantle flows (Horváth et al., 2015; Balázs et al., 2016; Fodor et al., 2021).

In the region of the northeastern Pannonian Basin, a complex tectonic setting was formed around 13–11 Ma (Fig. 12c). Previously, thrusting of deep-water flysch units occurred from the Oligocene and accelerated during the Early to Middle-Miocene resulting in a shortening of ~ 340 km (Roure et al., 1993; Nakapelyukh et al., 2018), coevally with subduction roll-back and the extension of the Pannonian Basin (Royden et al., 1982, 1983; Royden and Faccenna, 2018). Volcanism occurred close to the northeastern Carpathians thin-skinned fold-and-thrust belt, which is an accretionary prism developed along the convergence zone

~18–16 Ma: slab roll-back, lithosphere extension behind retreating subduction, rhyolitic ignimbrite flare-up



~16–13 Ma: slab roll-back, progressive lithosphere extension, ongoing large silicic explosive eruptions, andesite-dacite volcanism



~13–11 Ma: convergence terminated, final slab step-back, vertical slab descent, lithosphere extension/basin subsidence near the orogenic zone, andesite-rhyolite volcanism

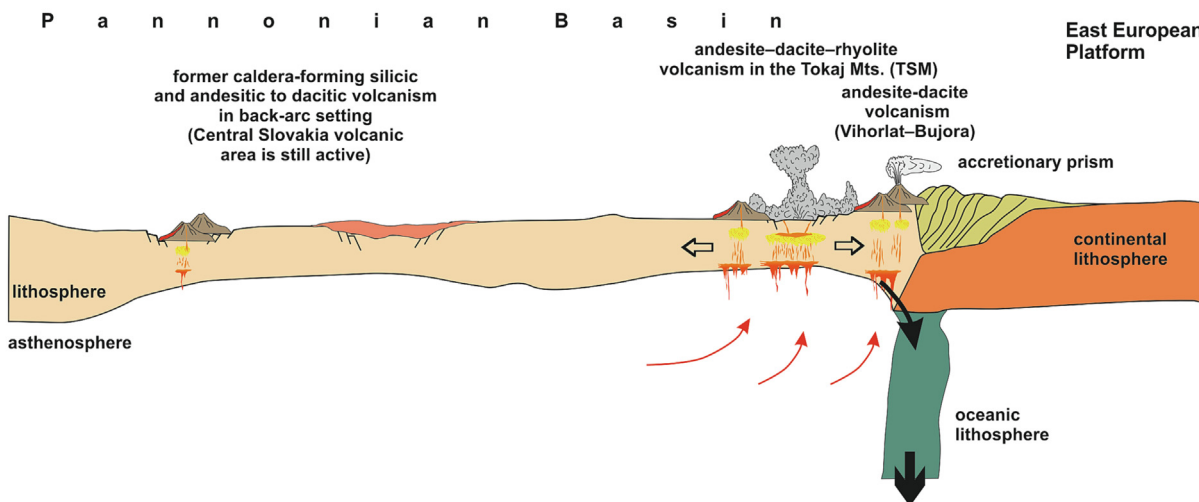


Fig. 12. Conceptual model for the origin of the TSM volcanism at the convergence zone between the Eurasian plate and the ALCAPA microplate of the Pannonian Basin. (a) 18–16 Ma: rhyolite ignimbrite flare-up, lithospheric extension behind the slab-rollback, retreating subduction (b) 16–13 Ma: Progressive lithospheric extension, slab-rollback, ongoing large silicic explosive events, andesite-dacite volcanism (c) 13–11 Ma: convergence terminated, final slab roll-back, vertical slab descent, lithospheric thinning near the orogenic zone, andesite-rhyolite volcanism.

between the East European Platform and the amalgamated ALCAPA–Tisza–Dacia domain (Horváth and Berckhemer, 1982; Csontos et al., 1992; Oszczytko et al., 2006). Based on tectonic observations, (U-Th)/He and fission track dating, contraction stopped in the external front of the wedge at around 12 Ma (Nakapelyukh et al., 2018; Roger et al., 2022). At that time, the frontal convergence terminated, and this probably led to steepening of the subducted slab, which reached a near-vertical position (Fig. 12c). The final back-stepping of the slab and its steepening could be connected to a major lithospheric thinning/extension phase just behind the accreted flysch units (e.g. Balázs et al., 2016). This is reflected by the very rapid subsidence and sedimentation in the Transcarpathian Depression including the East Slovakian Basin between 13.5 Ma and 11.6 Ma (ca. 3 km thick sedimentary pile; Rudinec, 1989; Kováč et al., 1995; Subová et al., 2022).

Accurate zircon U-Pb dating, Hf-isotope as well as trace element compositional data presented in this paper can help to understand better the reason of volcanism in this unusual setting, i.e. close vicinity to an orogenic convergence zone. Petrogenesis of the age-progressive silicic volcanism in the Bükkalja and the TM may reflect the evolution of the lithospheric thinning, subduction dynamics, i.e., the process of slab roll-back, the later slab steepening and the changing mantle flow dynamics (Fig. 12). The major rhyolitic ignimbrite flare-up between 18.1 Ma and 14.4 Ma was governed primarily by the lithosphere extension behind the retreating subduction zone (Fig. 12a, b; Lukács et al., 2018). The proposed ages of the explosive eruptions between 13.1 Ma and 11.6 Ma in the TM also notably coincide with progressive lithospheric thinning, but close to the subduction zone, during the last phase of orogenic convergence, termination of subduction and slightly predate the presumed slab detachment (Balázs et al., 2016; Nakapelyukh et al., 2018; Roger et al., 2022). Glass rare-earth element patterns as well as zircon trace element characteristics of the silicic explosive volcanic products suggest different magma type compared to most of the Bükkalja rhyolites (Fig. 11 and Supplementary Data, Sheet 3). The TM silicic magma was typically more reduced in redox state and possibly less hydrous ($H_2O < 4$ wt%). Such features are typical of extensional environments, i.e., at thinning lithosphere where the primary mafic melts are produced by near-adiabatic decompression melting in the mantle, in contrast to the subduction zones where wet and oxidized magmas are generated by hydrous melting (Bachmann and Bergantz, 2008). These contrasting characters can be reflected also in the evolved silicic magmas formed along distinct crystal fractionation paths governed by the water content of the magma. The Demjén and Eger ignimbrites in the Bükkalja volcanic field have a clear amphibole signature ('wet' magma differentiation), whereas rare earth element signature of the TM rhyolites implies strong plagioclase \pm pyroxene crystallization ('dry' magma differentiation). Such two magma types were described in the Taupo volcanic zone, where their presence was explained by variable fluid fluxes into the mantle (Deering et al., 2010). Accordingly, the 13.1–11.6 Ma TM silicic volcanism could have occurred at a magma generation environment characterized by relatively low fluid flux, which is consistent with the terminating subduction at the Carpathian orogenic zone, and it seems to be more plausible with a stronger connection to the ongoing lithospheric thinning at the northeastern margin of the Pannonian Basin and the passive upwelling of asthenospheric mantle. The Hf-isotope variation from strong negative to around zero values imply a decreasing crustal and/or increasing mantle component in the erupted magmas at about 12 Ma that strengthens the extension-related connection of the volcanism.

Tectonic features of the TSM, i.e. volcanism in a graben structure (Gyarmati, 1977) provides additional support to this interpre-

tation. Furthermore, presently there is a thin (about 70–80 km) lithosphere and high heat flow in this area that require a former massive extension process. While the early phase of extension of the TcB was accommodated by Early to Middle Miocene metamorphic core complex formation (Soták et al., 2000), later on (ca. 13–12 Ma), contemporaneously with the TM volcanism, further subsidence and extension occurred closely related to the dynamic changes during the terminating phase of the subduction, which modified the slab geometry and induced mantle flow (Fig. 12c). The last phase of the slab roll-back (from ca. 13.5 Ma), and the related mantle flow was followed by progressing slab steepening when the descending subducted lithosphere became almost vertical (from ca. 12 Ma). These processes could have exerted a pull in the lithosphere of the upper plate leading to thinning and accelerated subsidence as well as an uprise of the asthenospheric mantle near the steepening slab (TcB). This mantle reorganization could explain some of the geochemical signatures in the TM rhyolites, e.g., the prevailing 'hot-dry-reduced' magma character and the increasing mantle component in the erupted magmas at around 12 Ma. The tectonic situation could be similar what is going on currently at the Vrancea zone of southeastern Carpathians, Romania, where major subsidence occurs forming several basins above the vertically descending slab, which undergoes progressive detachment (Girbacea and Frisch, 1998; Wortel and Spakman, 2000; Tărâpoancă et al., 2004; Maţenco et al., 2007; 2022). Northern Borneo, Malaysia is another setting of subduction termination environment, where lithospheric drip was invoked as a driving process (Pilia et al., 2023). In summary, the large-volume explosive silicic volcanism in the TM provides an example of rhyolitic volcanism in a thinning continental lithosphere regime at the final stage of subduction.

7. Concluding remarks and perspectives for distal tephra correlations

In the Pannonian Basin, the 18.1–14.4 Ma silicic ignimbrite flare-up was followed by another notable period of rhyolitic volcanism. New zircon U-Pb dating suggests that this occurred between 13.1 and 11.5 Ma in the Tokaj Mts., where four major pyroclastic units were identified. Two of them were likely related to caldera collapse and resulted in large volume (presumably > 100 km³) of erupted volcanic material (the 13.1 Ma SAU and 12.0 Ma Szerencs eruptions), whereas the other two likely represent multiple smaller events. This volcanism was associated with rhyolitic extrusive activity as well as massive andesitic volcanism. The significant increase of ϵ Hf values in zircon with time implies that mantle-derived magmas became dominant, possibly along with progressive lithospheric thinning. This was likely related to the latest stage of subduction, when the vertically descending slab exerted suction in the overlying lower lithosphere. In the surrounding basin areas, such as in the Transcarpathian basin (e.g. Kaličiak and Žec, 1995; Vass et al., 2005), the Transylvanian basin as well as in the Carpathian foredeep, several Badenian to Sarmatian (14–11 Ma) tuff beds were recognized, but only few of them were dated even though they have great stratigraphic significance. De Leeuw et al., (2013, 2018) used Ar-Ar dating mostly on K-feldspar for tuffs from the Transylvanian basin and got ages such as 13.32 Ma, 12.37 Ma, among others. Vasiliev et al. (2010) dated the Oarba tuff and obtained 11.62 ± 0.04 Ma age. For the Slănic section, Eastern Carpathians, 13.32 Ma and 13.7 Ma Ar-Ar ages were published for two distinct tephra layers (Bojar et al., 2018; De Leeuw et al., 2018). In the Polish Carpathian Foredeep, the Badenian–Sarmatian sedimentary sections contain also several tuff layers, a few of them were already dated, resulted in 13.62 and 13.76 Ma (Bukowski et al., 2010) and

13.06 Ma ages (Śliwiński et al., 2012). Furthermore, Danišik et al. (2021) described a tephra layer (Gorelka tephra) in a palaeovalley of the Don river, southwestern Russia and dated to 11.5 ± 0.5 Ma by coupled U–Pb and U–Th/He method. They proposed that this volcanic material could be related to one of a gigantic eruptions in the Carpathian arc, although they were not able to find the proximal counterparts. This age strikingly fits with that determined for the Vizsoly ignimbrite, although the glass trace element compositions are distinct. The zircon fingerprint technique (Lukács et al., 2021), i.e. the combined use of U–Pb dates and trace element content of zircon grains could be a viable technique to correlate these tephra layers and construct a robust geochronological framework of large eruption events and distal volcanic material in the Carpathian-Pannonian region and its surroundings. Identification and documentation of eruption ages and trace element compositional characteristics of zircon, a resistant mineral phase, for various large rhyolitic eruptions in a time span from 18.1 Ma to 11.5 Ma (Lukács et al., 2015, 2018, 2021 and this study) is a promising tool to correlate these distal tephra layers and as a result constrain the ages of the host sediments.

CRedit authorship contribution statement

Réka Lukács: Conceptualization, Investigation, Formal analysis, Visualization, Writing – original draft, Funding acquisition. **Marcel Guillong:** Investigation, Writing – review & editing. **János Szepesi:** Investigation, Visualization. **Dawid Szymanowski:** Investigation, Visualization, Writing – review & editing. **Maxim Portnyagin:** Investigation, Writing – review & editing. **Sándor Józsa:** Investigation. **Olivier Bachmann:** Writing – review & editing. **Maurizio Petrelli:** Formal analysis. **Samuel Müller:** Investigation. **David Schiller:** Formal analysis. **László Fodor:** Writing – review & editing. **Cyril Chelle-Michou:** Resources. **Szabolcs Harangi:** Investigation, Visualization, Writing – review & editing, Funding acquisition.

Declaration of competing interest

The authors declare that they have no known competing financial interests or personal relationships that could have appeared to influence the work reported in this paper.

Acknowledgement

Members of the HUN-REN-ELTE Volcanology Research Group, especially Dóra Miklós, Eszter Mészáros, Zoltán Kovács and Péter Janka are thanked for their help in sample preparation. Mario Thöner (GEOMAR) is thanked for his assistance with electron microprobe analyses. We are grateful to the two anonymous reviewers to help improving our manuscript and also to the editor, Andrea Festa, for the careful handling of our submission.

Fund

This work was supported by the National Research, Development and Innovation Office–NKFIH, Hungary (OTKA FK131869, K134873). RL was supported by the Bolyai János Research Fellowship and MP and SM thank support from DFG project GA1960/14-1 (Germany) for funding LA-ICP-MS analyses. GEOMAR (Kiel, Germany) funded electron microprobe analyses.

Appendix A. Supplementary material

Supplementary data to this article can be found online at <https://doi.org/10.1016/j.gr.2024.01.004>.

References

- Allan, A.S.R., Barker, S.J., Millet, M.-A., Morgan, D.J., Rooyackers, S.M., Schipper, C.I., Wilson, C.J.N., 2017. A cascade of magmatic events during the assembly and eruption of a super-sized magma body. *Contribut. Mineral. Petrol.* 172, 49. <https://doi.org/10.1007/s00410-017-1367-8>.
- Anderson, A.T., Davis, A.M., Lu, F., 2000. Evolution of Bishop Tuff Rhyolitic magma based on melt and magnetite inclusions and zoned phenocrysts. *J. Petrol.* 41, 449–473. <https://doi.org/10.1093/petrology/41.3.449>.
- Arp, G., Dunkl, I., Jung, D., Karius, V., Lukács, R., Zeng, L., Reimer, A., Head, J.W., III, 2021. A Volcanic Ash Layer in the Nördlinger Ries Impact Structure (Miocene, Germany): Indication of Crater Fill Geometry and Origins of Long-Term Crater Floor Sagging. *J. Geophys. Res.-Planet.* 126. <https://doi.org/10.1029/2020JE006764>.
- Bachmann, O., Bergantz, G.W., 2004. On the origin of crystal-poor rhyolites: Extracted from batholithic crystal mushes. *J. Petrol.* 45, 1565–1582. <https://doi.org/10.1093/petrology/egh019>.
- Bachmann, O., Bergantz, G.W., 2008. Rhyolites and their source mushes across tectonic settings. *J. Petrol.* 49, 2277–2285. <https://doi.org/10.1093/petrology/egn068>.
- Bachmann, O., Huber, C., 2016. Silicic magma reservoirs in the Earth's crust. *Am. Mineral.* 101, 2377–2404. <https://doi.org/10.2138/am-2016-5675>.
- Bachmann, O., Oberli, F., Dungan, M.A., Meier, M., Mundil, R., Fischer, H., 2007. ⁴⁰Ar/³⁹Ar and U–Pb dating of the Fish Canyon magmatic system, San Juan Volcanic field, Colorado: Evidence for an extended crystallization history. *Chem. Geol.* 236, 134–166. <https://doi.org/10.1016/j.chemgeo.2006.09.005>.
- Bada, G., Horváth, F., 2001. On the structure and tectonic evolution of the Pannonian Basin and surrounding orogens. *Acta Geol. Hung.* 44, 301–327.
- Bada, G., Horváth, F., Dövényi, P., Szafián, P., Windhoffer, G., Cloetingh, S., 2007. Present-day stress field and tectonic inversion in the Pannonian basin. *Global Planet. Change.* 58, 165–180. <https://doi.org/10.1016/j.gloplacha.2007.01.007>.
- Balázs, A., Maţenco, L., Magyar, I., Horváth, F., Cloetingh, S., 2016. The link between tectonics and sedimentation in back-arc basins: New genetic constraints from the analysis of the Pannonian Basin. *Tectonics* 35, 1526–1559. <https://doi.org/10.1002/2015tc004109>.
- Balla, Z., 1984. The Carpathian loop and the Pannonian Basin: a kinematic analysis. *Geofiz. Közl.* 30, 313–353.
- Baráth, I., Kovács, M., Soták, J., Landkreijer, A., 1997. Tertiary collision, metamorphism and basin forming processes in the Eastern Slovakia (Central Western Carpathians). In: Grecula, P., Hovorka, D., Putis, M. (Eds.), *Geological evolution of the Western Carpathians*. Miner. Slov. Monograph, pp. 65–97.
- Bercea, R.I., Balc, R., Tamas, A., Filipescu, S., Tamas, D.M., Guillong, M., Szekely, S.F., Lukács, R., 2023. Insights into the palaeoenvironments, structure and stratigraphy of the lower Miocene of the Eastern Carpathians Bend Zone, Romania. *Geol. Q.* 62, 1–26. <https://doi.org/10.7306/gq.1673>.
- Bindeman, I.N., Valley, J.W., 2001. Low-delta O–18 rhyolites from Yellowstone: Magmatic evolution based on analyses of zircons and individual phenocrysts. *J. Petrol.* 42, 1491–1517. <https://doi.org/10.1093/petrology/42.8.1491>.
- Black, L.P., Kamo, S.L., Allen, C.M., Davis, D.W., Aleinikoff, J.N., Valley, J.W., Mundil, R., Campbell, I.H., Korsch, R.J., Williams, I.S., Foudoulis, C., 2004. Improved ²⁰⁶Pb/²³⁸U microprobe geochronology by the monitoring of a trace-element-related matrix effect; SHRIMP, ID–TIMS, ELA–ICP–MS and oxygen isotope documentation for a series of zircon standards. *Chem. Geol.* 205, 115–140. <https://doi.org/10.1016/j.chemgeo.2004.01.003>.
- Blundy, J., Cashman, K., 2001. Ascent-driven crystallisation of dacite magmas at Mount St Helens, 1980–1986. *Contribut. Mineral. Petrol.* 140, 631–650. <https://doi.org/10.1007/s004100000219>.
- Bodor, B., Fodor, L., 2013. Miocene structural evolution of the Hernád graben (NE Hungary) based on integrated seismic and outcrop data. *Occasional Papers of the Geol. Geophys. Inst. Hungary* 1, 11–13.
- Bojar, A.-V., Barbu, V., Wojtowicz, A., Bojar, H.-P., Hałas, S., Duliu, O.G., 2018. Miocene Slănic Tuff, Eastern Carpathians, Romania, in the Context of Badenian Salinity Crisis. *Geosciences* 8, 73.
- Bouvier, A., Vervoort, J.D., Patchett, P.J., 2008. The Lu–Hf and Sm–Nd isotopic composition of CHUR: Constraints from unequilibrated chondrites and implications for the bulk composition of terrestrial planets. *Earth Planet. Sc. Lett.* 273, 48–57. <https://doi.org/10.1016/j.epsl.2008.06.010>.
- Branney, M.J., Bonnicksen, B., Andrews, G.D.M., Ellis, B., Barry, T.L., McCurry, M., 2008. 'Snake River (SR)-type' volcanism at the Yellowstone hotspot track: distinctive products from unusual, high-temperature silicic super-eruptions. *B. Volcanol.* 70, 293–314. <https://doi.org/10.1007/s00445-007-0140-7>.
- Briek, M., Richard Tapster, S., Schindlbeck-Belo, J., Gaynor, S.P., Kutterolf, S., Hauff, F., Georgiev, S.V., Trinajstić, N., Šuica, S., Brčić, V., Wang, K.-L., Lee, H.-Y., Beier, C., Abersteiner, A.B., Mišur, I., Peytcheva, I., Kukoč, D., Németh, B., Trajanova, M., Balen, D., Guillong, M., Szymanowski, D., Lukács, R., 2023. Tracing widespread Early Miocene ignimbrite eruptions and petrogenesis at the onset of the Carpathian-Pannonian Region silicic volcanism. *Gondw. Res.* 116, 40–60. <https://doi.org/10.1016/j.gr.2022.12.015>.
- Brown, S.K., Crossweller, H.S., Sparks, R.S.J., Cottrell, E., Deligne, N.I., Guerrero, N.O., Hobbs, L., Kiyosugi, K., Loughlin, S.C., Siebert, L., Takarada, S., 2014. Characterisation of the Quaternary eruption record: analysis of the Large Magnitude Explosive Volcanic Eruptions (LaMEVE) database. *J. Appl. Volcanol.* 3, 5. <https://doi.org/10.1186/2191-5040-3-5>.
- Brown, S.J.A., Fletcher, I.R., 1999. SHRIMP U–Pb dating of the pre-eruption growth history of zircons from the 340 ka Whakamaru Ignimbrite, New Zealand:

- Evidence for >250 k.y. magma residence times. *Geology* 27, 1035–1038. [https://doi.org/10.1130/0091-7613\(1999\)027<1035:supdot>2.3.co;2](https://doi.org/10.1130/0091-7613(1999)027<1035:supdot>2.3.co;2).
- Bukowski, K., de Leeuw, A., Gonera, M., Kuiper, K.F., Krzywiac, P., Peryt, D., 2010. Badenian tuffite levels within the Carpathian orogenic front (Gdów-Bochnia area, Southern Poland): radioisotopic dating and stratigraphic position. *Geol. Q.* 54, 449–464.
- Camp, V.E., Wells, R.E., 2021. The case for a long-lived and robust Yellowstone hotspot. *GSA Today* 31, 4–10.
- Chamberlain, K.J., Wilson, C.J.N., Wooden, J.L., Charlier, B.L.A., Ireland, T.R., 2014. New perspectives on the Bishop Tuff from zircon textures, ages and trace elements. *J. Petrol.* 55, 395–426. <https://doi.org/10.1093/ptrology/egt072>.
- Charlier, B.L.A., Wilson, C.J.N., Lowenstern, J.B., Blake, S., Van Calsteren, P.W., Davidson, J.P., 2005. Magma generation at a large, hyperactive silicic Volcano (Taupo, New Zealand) revealed by U-Th and U-Pb systematics in zircons. *J. Petrol.* 46, 3–32. <https://doi.org/10.1093/ptrology/egh060>.
- Chernyshev, I.V., Konečný, V., Lexa, J., Kovalenker, V.A., Jeleň, S., Lebedev, V.A., Goltzman, Y.V., 2013. K-Ar and Rb-Sr geochronology and evolution of the Štiavnica Stratovolcano (Central Slovakia). *Geol. Carpath.* 64 (4), 327–351. <https://doi.org/10.2478/geoca-2013-0023>.
- Christiansen, E.H., 2005. Contrasting processes in silicic magma chambers: evidence from very large volume ignimbrites. *Geol. Mag.* 142, 669–681. <https://doi.org/10.1017/s0016756805001445>.
- Christiansen, R., Foulger, G., Evans, J., 2002. Upper-mantle origin of the Yellowstone Hotspot. *Geol. Soc. Amer. Bull.* 114, 1245–1256.
- Christiansen, E.H., McCurry, M., 2008. Contrasting origins of Cenozoic silicic volcanic rocks from the western Cordillera of the United States. *B. Volcanol.* 70, 251–267. <https://doi.org/10.1007/s00445-007-0138-1>.
- Christiansen, R.L., 1984. Yellowstone magmatic evolution: Its bearing on understanding large-volume explosive volcanism. In: *Explosive Volcanism, Its Inception, Evolution and Hazards*. In: National Research Council Studies in Geophysics. National Academy Press, Washington, D.C, pp. 84–95.
- Cole, J.W., 1990. Structural control and origin of volcanism in the Taupo volcanic zone, New Zealand. *B. Volcanol.* 52, 445–459. <https://doi.org/10.1007/bf00268925>.
- Csontos, L., 1995. Tertiary tectonic evolution of the Intra-Carpathian area: a review. *Acta Vulcanol.* 7, 1–13.
- Csontos, L., Nagymarosy, A., 1998. The Mid-Hungarian line: a zone of repeated tectonic inversions. *Tectonophysics* 297 (1–4), 51–71. [https://doi.org/10.1016/S0040-1951\(98\)00163-2](https://doi.org/10.1016/S0040-1951(98)00163-2).
- Csontos, L., Nagymarosy, A., Horváth, F., Kovács, M., 1992. Tertiary evolution of the Intra-Carpathian area: A model. *Tectonophysics* 208, 221–241. [https://doi.org/10.1016/0040-1951\(92\)90346-8](https://doi.org/10.1016/0040-1951(92)90346-8).
- Danišik, M., Ponomareva, V., Portnyagin, M., Popov, S., Zastrozhnov, A., Kirkland, C. L., Evans, N.J., Konstantinov, E., Hauff, F., Garbe-Schönberg, D., 2021. Gigantic eruption of a Carpathian volcano marks the largest Miocene transgression of Eastern Paratethys. *Earth Planet. Sc. Lett.* 563, <https://doi.org/10.1016/j.epsl.2021.116890>.
- Davies, G.R., Halliday, A.N., 1998. Development of the Long Valley rhyolitic magma system: strontium and neodymium isotope evidence from glasses and individual phenocrysts. *Geochim. Cosmochim. Ac.* 62, 3561–3574. [https://doi.org/10.1016/S0016-7037\(98\)00247-6](https://doi.org/10.1016/S0016-7037(98)00247-6).
- de Leeuw, A., Filipescu, S., Matenco, L., Krijgsman, W., Kuiper, K., Stoica, M., 2013. Paleomagnetic and chronostratigraphic constraints on the Middle to Late Miocene evolution of the Transylvanian Basin (Romania): Implications for Central Paratethys stratigraphy and emplacement of the Tisza-Dacia plate. *Global Planet. Change.* 103, 82–98. <https://doi.org/10.1016/j.gloplacha.2012.04.008>.
- de Leeuw, A., Tulbure, M., Kuiper, K.F., Melinte-Dobrinescu, M.C., Stoica, M., Krijgsman, W., 2018. New 40Ar/39Ar, magnetostratigraphic and biostratigraphic constraints on the termination of the Badenian Salinity Crisis: Indications for tectonic improvement of basin interconnectivity in Southern Europe. *Global Planet. Change.* 169, 1–15. <https://doi.org/10.1016/j.gloplacha.2018.07.001>.
- de Silva, S.L., 1989. Altiplano-Puna volcanic complex of the central Andes. *Geology* 17, 1102–1106. [https://doi.org/10.1130/0091-7613\(1989\)017<1102:apvcot>2.3.co;2](https://doi.org/10.1130/0091-7613(1989)017<1102:apvcot>2.3.co;2).
- Deering, C.D., Cole, J.W., Vogel, T.A., 2008. A Rhyolite Compositional Continuum Governed by Lower Crustal Source Conditions in the Taupo Volcanic Zone, New Zealand. *J. Petrol.* 49, 2245–2276. <https://doi.org/10.1093/ptrology/egn067>.
- Deering, C.D., Gravelly, D.M., Vogel, T.A., Cole, J.W., Leonard, G.S., 2010. Origins of cold-wet-oxidizing to hot-dry-reducing rhyolite magma cycles and distribution in the Taupo Volcanic Zone, New Zealand. *Contrib. Mineral. Petrol.* 160, 609–629. <https://doi.org/10.1007/s00410-010-0496-0>.
- Dombrádi, E., Sokoutis, D., Bada, G., Cloetingh, S., Horváth, F., 2010. Modelling recent deformation of the Pannonian lithosphere: Lithospheric folding and tectonic topography. *Tectonophysics* 484, 103–118. <https://doi.org/10.1016/j.tecto.2009.09.014>.
- Dövényi, P., Horváth, F., 1988. A review of temperature; thermal conductivity; heat flow data from the Pannonian basin. In: Royden, L., Horváth, F. (Eds.), *The Pannonian Basin, a Study in Basin Evolution*. American Association of Petroleum Geologists, Memoir 45, pp. 195–223.
- Downes, H., Pantó, G., Póka, T., Matthey, D.P., Greenwood, P.B., 1995. Calc-alkaline volcanics of the Inner Carpathian arc, Northern Hungary: new geochemical and oxygen isotopic results. In: Downes, H., Vaselli, O. (Eds.), *Neogene and Related Volcanism in the Carpatho-Pannonian Region*. *Acta Vulcanol.* pp. 29–41.
- Eddy, M.P., Ibañez-Mejía, M., Burgess, S.D., Coble, M.A., Cordani, U.G., DesOrmeau, J., Gehrels, G.E., Li, X., MacLennan, S., Pecha, M., Sato, K., Schoene, B., Valencia, V.A., Vervoort, J.D., Wang, T., 2019. GHR1 zircon – A new eocene natural reference material for microbeam U-Pb geochronology and Hf isotopic analysis of zircon. *Geostand. Geoanal. Res.* 43, 113–132. <https://doi.org/10.1111/ggr.12246>.
- Fodor, L., Jelen, B., Márton, E., Skaberne, D., Čar, J., Vrabec, M., 1998. Miocene-Pliocene tectonic evolution of the Slovenian Periadriatic fault: Implications for Alpine-Carpathian extrusion models. *Tectonics* 17, 690–709. <https://doi.org/10.1029/98tc01605>.
- Fodor, L., Csontos, L., Bada, G., Györfi, I., Benkovics, L., 1999. Tertiary tectonic evolution of the Pannonian Basin system and neighbouring orogens: a new synthesis of palaeostress data. *Geol. Soc. London. Spec. Pub.* 156, 295–334. <https://doi.org/10.1144/gsl.sp.1999.156.01.15>.
- Fodor, L., Radócz, G., Sztanó, O., Koroknai, B., Csontos, L., Harangi, S., 2005. Postconference excursion: tectonics, sedimentation and magmatism along the Darnó Zone. *Geoinfo* 19, 142–162.
- Fodor, L., Balázs, A., Csillag, G., Dunkl, I., Héja, G., Jelen, B., Kelemen, P., Kövér, S., Németh, A., Nyíri, D., Selmececi, I., Trajanova, M., Vrabec, M., Vrabec, M., 2021. Crustal exhumation and decelerated migration from the Alpine orogenic margin towards the Pannonian extensional back-arc basin controlled by inheritance. *Global Planet. Change.* 201, <https://doi.org/10.1016/j.gloplacha.2021.103475>.
- Gansecki, C.A., Mahood, G.A., McWilliams, M., 1998. New ages for the climactic eruptions at Yellowstone: Single-crystal 40Ar/39Ar dating identifies contamination. *Geology* 26, 343–346. [https://doi.org/10.1130/0091-7613\(1998\)026<0343:naftce>2.3.co;2](https://doi.org/10.1130/0091-7613(1998)026<0343:naftce>2.3.co;2).
- Girbacea, R., Frisch, W., 1998. Slab in the wrong place: Lower lithospheric mantle delamination in the last stage of the Eastern Carpathian subduction retreat. *Geology* 26, 611–614. [https://doi.org/10.1130/0091-7613\(1998\)026<0611:sitwpl>2.3.co;2](https://doi.org/10.1130/0091-7613(1998)026<0611:sitwpl>2.3.co;2).
- Gravelly, D.M., Deering, C.D., Leonard, G.S., Rowland, J.V., 2016. Ignimbrite flare-ups and their drivers: A New Zealand perspective. *Earth-Sci. Rev.* 162, 65–82. <https://doi.org/10.1016/j.earscirev.2016.09.007>.
- Griffin, W., Powell, W., Pearson, N.J., O'Reilly, S., 2008. GLITTER: data reduction software for laser ablation ICP-MS. *Short Course Ser.* 40, 308–311.
- Grimes, C.B., John, B.E., Kelemen, P.B., Mazdab, F.K., Wooden, J.L., Cheadle, M.J., Hanghøj, K., Schwartz, J.J., 2007. Trace element chemistry of zircons from oceanic crust: A method for distinguishing detrital zircon provenance. *Geology* 35, 643–646. <https://doi.org/10.1130/g23603a.1>.
- Grimes, C.B., Wooden, J.L., Cheadle, M.J., John, B.E., 2015. "Fingerprinting" tectono-magmatic provenance using trace elements in igneous zircon. *Contrib. Mineral. Petrol.* 170, 46. <https://doi.org/10.1007/s00410-015-1199-3>.
- Gutiérrez, F., Payacán, I., Szymanowski, D., Guillong, M., Bachmann, O., Parada, M.A., 2018. Lateral magma propagation during the emplacement of La Gloria Pluton, central Chile. *Geology* 46, 1051–1054. <https://doi.org/10.1130/g45361.1>.
- Gyarmati, P., 1977. A Tokaji-hegység intermedier vulkanizmus. *Annal. Inst. Geol. Publ. Hung. LVII* 1, 196.
- Gyarmati, P., Perlaki, E., Pentelényi, L., 1976. A Tokaji-hegység földtani térképe – MÁFI Budapest.
- Halliday AN, Davidson JP, Hildreth W, Holden P (1991). Modelling the petrogenesis of high Rb/Sr silicic magmas. *Chem. Geol.* 92, 107–114. [https://doi.org/10.1016/0009-2541\(91\)90051-R](https://doi.org/10.1016/0009-2541(91)90051-R).
- Handy, M.R., Ustaszewski, K., Kissling, E., 2015. Reconstructing the Alps-Carpathians-Dinarides as a key to understanding switches in subduction polarity, slab gaps and surface motion. *Int. J. Earth Sci.* 104, 1–26. <https://doi.org/10.1007/s00531-014-1060-3>.
- Harangi, S., 2001. Neogene to Quaternary Volcanism of the Carpathian-Pannonian Region – a review. *Acta Geol. Hung.* 44, 223–258.
- Harangi, S., Lenkey, L., 2007. Genesis of the Neogene to Quaternary volcanism in the Carpathian-Pannonian region: Role of subduction, extension, and mantle plume. *Geol. S. Am.* 5, 418, 67–92. [https://doi.org/10.1130/2007.2418\(04\)](https://doi.org/10.1130/2007.2418(04)).
- Harangi, S., Wilson, M., Tonarini, S., 1995. Petrogenesis of Neogene potassic volcanic rocks in the Pannonian Basin. *Acta Vulcanol.* 7, 125–134.
- Harangi, S., Downes, H., Kósa, L., Szabó, C., Thirlwall, M.F., Mason, P.R.D., Matthey, D., 2001. Almandine garnet in calc-alkaline volcanic rocks of the Northern Pannonian Basin (Eastern-Central Europe): Geochemistry, petrogenesis and geodynamic implications. *J. Petrol.* 42, 1813–1843. <https://doi.org/10.1093/ptrology/42.10.1813>.
- Harangi, S., Mason, P.R.D., Lukács, R., 2005. Correlation and petrogenesis of silicic pyroclastic rocks in the Northern Pannonian Basin, Eastern-Central Europe: In situ trace element data of glass shards and mineral chemical constraints. *J. Volcanol. Geoth. Res.* 143, 237–257. <https://doi.org/10.1016/j.jvolgeores.2004.11.012>.
- Harangi, S., Downes, H., Thirlwall, M., Gmélung, K., 2007. Geochemistry, petrogenesis and geodynamic relationships of miocene calc-alkaline volcanic rocks in the Western Carpathian Arc, Eastern Central Europe. *J. Petrol.* 48, 2261–2287. <https://doi.org/10.1093/ptrology/egm059>.
- Harangi, S., Jankovics, M.É., Sági, T., Kiss, B., Lukács, R., Soós, I., 2015. Origin and geodynamic relationships of the Late Miocene to Quaternary alkaline basalt volcanism in the Pannonian basin, eastern-central Europe. *Int. J. Earth Sci.* 104, 2007–2032. <https://doi.org/10.1007/s00531-014-1105-7>.
- Hegedűs, E., Posgay, K., Bodoky, T., Fancsik, T., Kovács, A.C., Csabafi, R., Celebration Working Group 2002. 3D refraction tomographic images from the Mátra-Zemplén region. *Geol. Carpath. Spec. Issue* 53, Paper 158

- Hildreth, W., 1981. Gradients in silicic magma chambers: Implications for lithospheric magmatism. *J. Geophys. Res.-Sol. Ea.* 86, 10153–10192. <https://doi.org/10.1029/JB086B11p10153>.
- Hildreth, W., 2004. Volcanological perspectives on Long Valley, Mammoth Mountain, and Mono Craters: several contiguous but discrete systems. *J. Volcanol. Geoth. Res.* 136, 169–198. <https://doi.org/10.1016/j.jvolgeores.2004.05.019>.
- Horstwood, M.S.A., Košler, J., Gehrels, G., Jackson, S.E., McLean, N.M., Paton, C., Pearson, N.J., Sircombe, K., Sylvester, P., Vermeesch, P., Bowring, J.F., Condon, D. J., Schoene, B., 2016. Community-Derived Standards for LA-ICP-MS U-(Th)-Pb Geochronology – Uncertainty Propagation, Age Interpretation and Data Reporting. *Geostand. Geoanal. Res.* 40, 311–332. <https://doi.org/10.1111/j.1751-908X.2016.00379.x>.
- Horváth, F., 1993. Towards a mechanical model for the formation of the Pannonian basin. *Tectonophysics* 226, 333–357. [https://doi.org/10.1016/0040-1951\(93\)90126-5](https://doi.org/10.1016/0040-1951(93)90126-5).
- Horvath, F., Berckhemer, H., 1982. Mediterranean Backarc Basins. In: Berckhemer, H., Hsü, K. (Eds.). *Alpine-Mediterranean Geodynamics* 7, 141–173. <https://doi.org/10.1029/GD007p0141>.
- Horváth, F., Cloetingh, S., 1996. Stress-induced late-stage subsidence anomalies in the Pannonian basin. *Tectonophysics* 266, 287–300. [https://doi.org/10.1016/S0040-1951\(96\)00194-1](https://doi.org/10.1016/S0040-1951(96)00194-1).
- Horváth, F., Bada, G., Szafián, P., Tari, G., Ádám, A., Cloetingh, S., 2006. Formation and deformation of the Pannonian Basin: constraints from observational data. *Geol. Soc. Lond. Mem.* 32, 191–206. <https://doi.org/10.1144/gsl.mem.2006.032.01.11>.
- Horváth, F., Musitz, B., Balázs, A., Végh, A., Uhrin, A., Nádor, A., Koroknai, B., Pap, N., Tóth, T., Wörum, G., 2015. Evolution of the Pannonian basin and its geothermal resources. *Geothermics* 53, 328–352. <https://doi.org/10.1016/j.geothermics.2014.07.009>.
- Horvath, F., Stegena, L., Berckhemer, H., Coulon, C., Vine Frederick, J., Smith Austin, G., 1981. Models of Mediterranean back-arc basin formation. *Phil. T. R. Soc. A.* 300, 383–402. <https://doi.org/10.1098/rsta.1981.0071>.
- Houghton, B.F., Wilson, C.J.N., McWilliams, M.O., Lanphere, M.A., Weaver, S.D., Briggs, R.M., Pringle, M.S., 1995. Chronology and dynamics of a large silicic magmatic system: Central Taupo Volcanic Zone, New Zealand. *Geology* 23, 13–16. [https://doi.org/10.1130/0091-7613\(1995\)023<0013:caoaol>2.3.co;2](https://doi.org/10.1130/0091-7613(1995)023<0013:caoaol>2.3.co;2).
- Huang, H.-H., Lin, F.-C., Schmandt, B., Farrell, J., Smith, R.B., Tsai, V.C., 2015. The Yellowstone magmatic system from the mantle plume to the upper crust. *Science* 348, 773–776. <https://doi.org/10.1126/science.aaa5648>.
- Hughes, G.R., Mahood, G.A., 2011. Silicic calderas in arc settings: Characteristics, distribution, and tectonic controls. *GSA Bull.* 123, 1577–1595. <https://doi.org/10.1130/b30232.1>.
- Jackson, S.E., Pearson, N.J., Griffin, W.L., Belousova, E.A., 2004. The application of laser ablation-inductively coupled plasma-mass spectrometry to in situ U-Pb zircon geochronology. *Chem. Geol.* 211, 47–69. <https://doi.org/10.1016/j.chemgeo.2004.06.017>.
- Jaffey, A.H., Flynn, K.F., Glendenin, L.E., Bentley, W.C., Essling, A.M., 1971. Precision measurement of half-lives and specific activities of ²³⁵U and ²³⁸U. *Phys. Rev. C* 4 (5), 1889–1906.
- Jochum, K.P., Stoll, B., Herwig, K., Willbold, M., Hofmann, A.W., Amini, M., Aarburg, S., Abouchami, W., Hellebrand, E., Mocek, B., Raczek, I., Stracke, A., Alard, O., Bouman, C., Becker, S., Dücking, M., Brätz, H., Klemm, R., de Bruin, D., Canil, D., Cornell, D., de Hoog, C.-J., Dalpé, C., Danyushevsky, L., Eisenhauer, A., Gao, Y., Snow, J.E., Groschopf, N., Günther, D., Latkoczy, C., Guillong, M., Hauri, E.H., Höfer, H.E., Lahaye, Y., Horz, K., Jacob, D.E., Kasemann, S.A., Kent, A.J.R., Ludwig, T., Zack, T., Mason, P.R.D., Meixner, A., Rosner, M., Misawa, K., Nash, B.P., Pfänder, J., Premo, W.R., Sun, W.D., Tiepolo, M., Vannucci, R., Vennemann, T., Wayne, D., Woodhead, J.D., 2006. MPI-DING reference glasses for in situ microanalysis: New reference values for element concentrations and isotope ratios. *Geochim. Geophys. Geosyst.* 7. <https://doi.org/10.1029/2005GC001060>.
- Johannes, W., Holtz, F., 1996. The haplogranite system Qz-Ab-Or. In: Johannes, W., Holtz, F. (Eds.), *Petrogenesis and Experimental Petrology of Granitic Rocks*. Springer, Berlin Heidelberg, Berlin, Heidelberg, pp. 18–57. https://doi.org/10.1007/978-3-642-61049-3_2.
- Kaličiak, M., Žec, B., 1995. Review of Neogene volcanism of Eastern Slovakia. *Acta Vulcanol.* 7, 87–96.
- Kalmár, D., Hetényi, G., Balázs, A., Bondár, I. AlArray Working Group, 2021. Crustal thinning from orogen to back-arc basin: The structure of the Pannonian Basin region revealed by P-to-S converted seismic waves. *J. Geophys. Res.-Sol. Ea.* 126, (7). <https://doi.org/10.1029/2020JB021309> e2020JB021309.
- Kalmár, D., Petrescu, L., Stipčević, J., Balázs, A., Kovács, J., AlArrayPACASE Working Groups, 2023. Lithospheric Structure of the Circum-Pannonian Region Imaged by S-To-P Receiver Functions. *Geochemistry, Geophysics, Geosystems* 24. <https://doi.org/10.1029/2023GC010937> e2023GC010937.
- Karátson, D., Biró, T., Portnyagin, M., Kiss, B., Paquette, J.-L., Cseri, Z., Hencz, M., Németh, K., Lahitte, P., Márton, E., Kordos, L., Józsa, S., Hably, L., Müller, S., Szarvas, I., 2022. Large-magnitude (VEI ≥ 7) 'wet' explosive silicic eruption preserved a Lower Miocene habitat at the Ipolytarnóc Fossil Site. *North Hungary. Sci. Rep.* 12, 9743. <https://doi.org/10.1038/s41598-022-13586-3>.
- Kázmér, M., Kovács, S., 1985. Permian-Paleogene paleogeography along the eastern part of the Insubric-Periadriatic lineament system: Evidence for continental escape of the Bakony-Drauzug unit. *Acta Geol. Hung.* 28, 71–84.
- Keller, F., Bachmann, O., Geshi, N., Miyakawa, A., 2021. The Role of Crystal Accumulation and Cumulate Remobilization in the Formation of Large Zoned Ignimbrites: Insights From the Aso-4 Caldera-forming Eruption, Kyushu, Japan. *Front. Earth. Sci.* 8. <https://doi.org/10.3389/feart.2020.614267>.
- Keller, C.B., Schoene, B., Samperton, K.M., 2018. A stochastic sampling approach to zircon eruption age interpretation. *Geochem. Persp. Lett.* 8, 31–35. <https://doi.org/10.7185/geochemlet.1826>.
- Kennedy, A., Wotzlaw, J.-F., Crowley, J., Schmitz, M., Schaltegger, U., 2014. Eocene zircon reference material for microanalysis of U-Th-Pb isotopes and trace elements. *Can. Mineral.* 52, 409–421. <https://doi.org/10.3749/canmin.52.3.409>.
- Kiss, P., Gmélinc, K., Molnár, F., Pécskay, Z., 2010. Geochemistry of Sarmatian volcanic rocks in the Tokaj Mts (NE Hungary) and their relationship to hydrothermal mineralization. *Cent. Europ. Geol.* 53, 377–403. <https://doi.org/10.1556/CEUgeol.53.2010.4.3>.
- Klemetti, E.W., Deering, C.D., Cooper, K.M., Roeske, S.M., 2011. Magmatic perturbations in the Okataina Volcanic Complex, New Zealand at thousand-year timescales recorded in single zircon crystals. *Earth Planet. Sc. Lett.* 305, 185–194. <https://doi.org/10.1016/j.epsl.2011.02.054>.
- Kohút, M., Anczkiewicz, R., Biron, A., Mikuš, T., Milovska, S., Milovský, R., Surka, J., Danišik, M., Kirkland, C., Erban, V., Kočergina, Y., Magna, T., Gerdes, A., Halton, A., Sherlock, S., Jesenak, K., Pearce, N., Recio, C., Westgate, J., Baco, P., 2019. Genesis of the Carpathian obsidians. *Geol. Carp.* 70, 75–78.
- Kohút, M., Sherlock, S.C., Halton, A.M., 2021. The 40Ar-39Ar dating and geochemistry of the Carpathian C1 obsidians (Zemplín, Slovakia). *Geol. Carp.* 72 (4), 344–357. <https://doi.org/10.31577/GeolCarp.72.4.5>.
- Konečný, V., Kováč, M., Lexa, J., Šefara, J., 2002. Neogene evolution of the Carpatho-Pannonian region: an interplay of subduction and backarc diapiric uprise in the mantle. *Eur. Geophys. Union Stephan Mueller Spec. Publ. Ser.* 1, 105–123.
- Kováč, M., Kováč, P., Marko, F., Karoli, S., Janočko, J., 1995. The East Slovakian Basin – A complex back-arc basin. *Tectonophysics* 252, 453–466. [https://doi.org/10.1016/0040-1951\(95\)00183-2](https://doi.org/10.1016/0040-1951(95)00183-2).
- Kováč, M., Andreyeva-Grigorovich, A., Bajraktarević, Z., Brzobohatý, R., Filipescu, S., Fodor, L., Harzhauser, M., Oszczypko, N., Pavelic, D., Rögl, F., Saftić, B., Sliva, L., Studencka, B., 2007. Badenian evolution of the Central Paratethys sea: paleogeography, climate and eustatic sea level changes. *Geol. Carp.* 58, 579–606.
- Kováč, M., Halasova, E., Hudáčková, N., Holcová, K., Hyžný, M., Jamrich, M., Ruman, A.I., 2018. Towards better correlation of the Central Paratethys regional time scale with the standard geological time scale of the Miocene Epoch. *Geol. Carp.* 69, 283–300. <https://doi.org/10.1515/geoca-2018-0017>.
- Kovacs, M., Seghedi, L., Yamamoto, M., Fülöp, A., Pécskay, Z., Jurje, M., 2017. Miocene volcanism in the Oaş-Gutâi Volcanic Zone, Eastern Carpathians, Romania: Relationship to geodynamic processes in the Transcarpathian Basin. *Lithos* 294–295, 304–318. <https://doi.org/10.1016/j.lithos.2017.09.027>.
- Lenkey, L., Dövényi, P., Horvath, F., Cloetingh, S., 2002. Geothermics of the Pannonian basin and its bearing on the neotectonics. *Stephan Mueller Spec. Publ. Ser.* 3, 29–40. <https://doi.org/10.5194/smssps-3-29-2002>.
- Lexa, J., Bačo, P., Bačová, Z., Konečný, P., Konečný, V., Németh, K., Pécskay, Z., 2014. Evolution of monogenetic rhyolite volcanoes: Viničky, Eastern Slovakia. *Bul. Shk. Geol.* 1/2014, Special Issue, Proceedings of XX CBGA Congress, Tirana, Albania, SS12, 234–237.
- Lexa, J., Seghedi, L., Németh, K., Szakács, A., Konečný, V., Pécskay, Z., Fülöp, A., Kovacs, M., 2010. Neogene-Quaternary Volcanic forms in the Carpathian-Pannonian region: a review. *Open Geosci.* 2, 207–270. <https://doi.org/10.2478/v10085-010-0024-5>.
- Loader, M.A., Wilkinson, J.J., Armstrong, R.M., 2017. The effect of titanite crystallisation on Eu and Ce anomalies in zircon and its implications for the assessment of porphyry Cu deposit fertility. *Earth Planet. Sc. Lett.* 472, 107–119. <https://doi.org/10.1016/j.epsl.2017.05.010>.
- Lukács, R., Harangi, S., Bachmann, O., Guillong, M., Danišik, M., Buret, Y., von Quadt, A., Dunkl, I., Fodor, L., Sliwinski, J., Soós, I., Szepesi, J., 2015. Zircon geochronology and geochemistry to constrain the youngest eruption events and magma evolution of the Mid-Miocene ignimbrite flare-up in the Pannonian Basin, eastern central Europe. *Contrib. Mineral. Petrol.* 170, 52. <https://doi.org/10.1007/s00410-015-1206-8>.
- Lukács, R., Guillong, M., Sliwinski, J., Dunkl, I., Bachmann, O., Harangi, S., 2018. LA-ICP-MS U-Pb zircon geochronology data of the Early to Mid-Miocene syn-extensional massive silicic volcanism in the Pannonian Basin (East-Central Europe). *Data Brief* 19, 506–513. <https://doi.org/10.1016/j.dib.2018.05.013>.
- Lukács, R., Harangi, S., Guillong, M., Bachmann, O., Fodor, L., Buret, Y., Dunkl, I., Sliwinski, J., von Quadt, A., Peytcheva, I., Zimmerer, M., 2018. Early to Mid-Miocene syn-extensional massive silicic volcanism in the Pannonian Basin (East-Central Europe): Eruption chronology, correlation potential and geodynamic implications. *Earth-Sci. Rev.* 179, 1–19. <https://doi.org/10.1016/j.earscirev.2018.02.005>.
- Lukács, R., Guillong, M., Bachmann, O., Fodor, L., Harangi, S., 2021. Tephrostratigraphy and magma evolution based on combined zircon trace element and U-Pb age data: Fingerprinting Miocene silicic pyroclastic rocks in the Pannonian Basin. *Front. Earth. Sci.* 9. <https://doi.org/10.3389/feart.2021.615768>.
- Lukács, R., Harangi, S., Gál, P., Szepesi, J., Di Capua, A., Norini, G., Sulpizio, R., Groppelli, G., Fodor, L., 2022. Formal definition and description of lithostratigraphic units related to the Miocene silicic pyroclastic rocks outcropping in Northern Hungary: A revision. *Geol. Carp.* 73, 137–158. <https://doi.org/10.31577/GeolCarp.73.2.3>.
- Mason, B.G., Pyle, D.M., Oppenheimer, C., 2004. The size and frequency of the largest explosive eruptions on Earth. *B. Volcanol.* 66, 735–748. <https://doi.org/10.1007/s00445-004-0355-9>.
- Maţenco, L., Bertotti, G., 2000. Tertiary tectonic evolution of the external East Carpathians (Romania). *Tectonophysics* 316, 255–286.

- Matenco, L., Bertotti, G., Leever, K., Cloetingh, S., Schmid, S.M., Tărăoancă, M., Dinu, C. (2007). Large-scale deformation in a locked collisional boundary: Interplay between subsidence and uplift, intraplate stress, and inherited lithospheric structure in the late stage of the SE Carpathians evolution. *Tectonics*, 26, TC4011, doi:10.1029/2006TC001951.
- Matenco, L., Radivojević, D., 2012. On the formation and evolution of the Pannonian Basin: Constraints derived from the structure of the junction area between the Carpathians and Dinarides. *Tectonics* 31. <https://doi.org/10.1029/2012TC003206>.
- Mattenco, L., Balázs, A., Nader, F.H., Haq, B.U., Fodor, L., 2022. Advances in the understanding of multi-scale and coupled evolution of orogens, sedimentary basins and the underlying lithosphere. *Global Planet. Change*, 208. <https://doi.org/10.1016/j.gloplacha.2021.103689>
- Mattinson, J.M., 2005. Zircon U-Pb chemical abrasion ("CA-TIMS") method: Combined annealing and multi-step partial dissolution analysis for improved precision and accuracy of zircon ages. *Chem. Geol.* 220, 47–66. <https://doi.org/10.1016/j.chemgeo.2005.03.011>.
- Miller, C.F., McDowell, S.M., Mapes, R.W., 2003. Hot and cold granites? Implications of zircon saturation temperatures and preservation of inheritance. *Geology* 31, 529–532. [https://doi.org/10.1130/0091-7613\(2003\)031<0529:hacgio>2.0.co;2](https://doi.org/10.1130/0091-7613(2003)031<0529:hacgio>2.0.co;2).
- Nakapelyukh, M., Bubiñak, I., Bubiñak, A., Jonckheere, R., Ratschbacher, L., 2018. Cenozoic structural evolution, thermal history, and erosion of the Ukrainian Carpathians fold-thrust belt. *Tectonophysics* 722, 197–209. <https://doi.org/10.1016/j.tecto.2017.11.009>.
- Nemčok, M., Pospisil, L., Lexa, J., Donelick, R.A., 1998. Tertiary subduction and slab break-off model of the Carpathian-Pannonian region. *Tectonophysics* 295, 307–340. [https://doi.org/10.1016/S0040-1951\(98\)00092-4](https://doi.org/10.1016/S0040-1951(98)00092-4).
- Németh, K., Pécskay, Z., Martin, U., Gmeling, K., Molnár, F., Cronin, S.J., 2008. Hyaloclastites, peperites and soft-sediment deformation textures of a shallow subaqueous Miocene rhyolitic dome-cryptodome complex, Pálháza, Hungary. *Geol. Soc., London Spec. Publ.* 302, 63–86. <https://doi.org/10.1144/SP302.5>.
- Oszczypko, N., Krzywiec, P., Popadyuk, I., Peryt, T., Golonka, J., Picha, F.J., 2006. Carpathian Foredeep Basin (Poland and Ukraine): Its Sedimentary, Structural, and Geodynamic Evolution. In: Golonka, J., Picha, F.J. (Eds.), *The Carpathians and Their Foreland: Geology and Hydrocarbon Resources*. AAPG. <https://doi.org/10.1306/985612m843072>.
- Papale, P., Marzocchi, W., 2019. Volcanic threats to global society. *Science* 363, 1275–1276. <https://doi.org/10.1126/science.aaw7201>.
- Paton, C., Hellstrom, J., Paul, B., Woodhead, J., Hergt, J., 2011. Iolite: Freeware for the Visualisation and Processing of Mass Spectrometric Data. *J. Anal. At. Spectrom.* VL – IS, online. doi:10.1039/C1JA10172B.
- Pearce, N.J.G., Westgate, J.A., Gualda, G.A.R., Gatti, E., Muhammad, R.F., 2020. Tephra glass chemistry provides storage and discharge details of five magma reservoirs which fed the 75 ka Youngest Toba Tuff eruption, northern Sumatra. *J. Quaternary Sci.* 35, 256–271. <https://doi.org/10.1002/jqs.3149>.
- Pécskay, Z., Balogh, K., Szeky-Fux, V., Gyarmati, P., 1986. Geochronological investigations of the Neogene volcanism of the Tokaj Mountains. *Geol. Zbornik*, 37, 635–655.
- Pécskay, Z., Molnár, F., 2002. Relationships between volcanism and hydrothermal activity in the Tokaj Mountains, Northeast Hungary, based on K-Ar ages. *Geol. Carpath.* 53, 303–314.
- Pécskay, Z., Balogh, K., Székely, F.V., Gyarmati, P., 1987. A Tokaji-hegység miocén vulkánosságának K/Ar geokronológiája. *Földt. Közl.* 117, 237–253.
- Pécskay, Z., Seghedi, I., Downes, H., Prychodko, M., Mackiv, B., 2000. K/Ar dating of Neogene calc-alkaline volcanic rocks from Transcarpathian Ukraine. *Geol. Carpath.* 51, 83–89.
- Pécskay, Z., Lexa, J., Szakács, A., Seghedi, I., Balogh, K., Konecny, V., Zelenka, T., Kovacs, M., Poka, T., Fulop, A., Marton, E., Panaiotu, C., Cvetkovic, V., 2006. Geochronology of Neogene magmatism in the Carpathian arc and intra-Carpathian area. *Geol. Carpath.* 57, 511–530.
- Petrus, J.A., Kamber, B.S., 2012. *VizualAge*: A novel approach to laser ablation ICP-MS U-Pb geochronology data reduction. *Geostand. Geoanal. Res.* 36, 247–270. <https://doi.org/10.1111/j.1751-908X.2012.00158.x>.
- Pettko, T., Halter, W.E., Webster, J.D., Aigner-Torres, M., Heinrich, C.A., 2004. Accurate quantification of melt inclusion chemistry by LA-ICP-MS: a comparison with EMP and SIMS and advantages and possible limitations of these methods. *Lithos* 78, 333–361. <https://doi.org/10.1016/j.lithos.2004.06.011>.
- Pilia, S., Davies, D.R., Hall, R., Bacon, C.A., Gilligan, A., Greenfield, T., Tongkul, F., Kramer, S.C., Wilson, C.R., Ghelichkhan, S., Cornwell, D.G., Colli, L., Rawlinson, N., 2023. Post-subduction tectonics induced by extension from a lithospheric drip. *Nat. Geosci.* 16, 646–652. <https://doi.org/10.1038/s41561-023-01201-7>.
- Piller, W.E., Harzhauser, M., Mandic, O., 2007. *Miocene Central Paratethys stratigraphy – current status and future directions*. *Stratigraphy* 4, 151–168.
- Portnyagin, M.V., Ponomareva, V.V., Zelenin, E.A., Bazanova, L.I., Pevzner, M.M., Pleychova, A.A., Rogozin, A.N., Garbe-Schönberg, D., 2020. TephraKam: geochemical database of glass compositions in tephra and welded tuffs from the Kamchatka volcanic arc (northwestern Pacific). *Earth Syst. Sci. Data* 12, 469–486. <https://doi.org/10.5194/essd-12-469-2020>.
- Ratschbacher, L., Merle, O., Davy, P., Cobbold, P., 1991a. Lateral extrusion in the eastern Alps, Part 1: Boundary conditions and experiments scaled for gravity. *Tectonics* 10, 245–256. <https://doi.org/10.1029/90TC02622>.
- Ratschbacher, L., Frisch, W., Linzer, H.-G., Merle, O., 1991b. Lateral extrusion in the eastern Alps, Part 2: Structural analysis. *Tectonics* 10, 257–271. <https://doi.org/10.1029/90TC02623>.
- Roger, M., de Leeuw, A., van der Beek, P., Husson, L., Sobel, E.R., Glodny, J., Bernet, M., 2022. Construction of the Ukrainian Carpathian Wedge from low-temperature thermochronology and tectono-stratigraphic analysis. *Egusphere* 2022, 1–44. <https://doi.org/10.5194/egusphere-2022-828>.
- Roure, F., Roca, E., Sassi, W., 1993. The Neogene evolution of the outer Carpathian flysch units (Poland, Ukraine and Romania): kinematics of a foreland/fold-and-thrust belt system. *Sed. Geol.* 86, 177–201. [https://doi.org/10.1016/0037-0738\(93\)90139-V](https://doi.org/10.1016/0037-0738(93)90139-V).
- Rowland, J.V., Wilson, C.J.N., Gravley, D.M., 2010. Spatial and temporal variations in magma-assisted rifting, Taupo Volcanic Zone, New Zealand. *J. Volcanol. Geoth. Res.* 190, 89–108. <https://doi.org/10.1016/j.jvolgeores.2009.05.004>.
- Royden, L., Faccenna, C., 2018. Subduction Orogeny and the Late Cenozoic Evolution of the Mediterranean Arcs. *Annu. Rev. Earth Pl. Sc.* 46, 261–289. <https://doi.org/10.1146/annurev-earth-060115-012419>.
- Royden, L.H., Horváth, F., Burchfiel, B.C., 1982. Transform faulting, extension, and subduction in the Carpathian Pannonian region. *Geol. Soc. Am. Bull.* 93, 717–725. [https://doi.org/10.1130/0016-7606\(1982\)93<717:TFEASi>2.0.CO;2](https://doi.org/10.1130/0016-7606(1982)93<717:TFEASi>2.0.CO;2).
- Royden, L., Horváth, F., Rumpler, J., 1983. Evolution of the Pannonian Basin System: 1. Tectonics. *Tectonics* 2, 63–90. <https://doi.org/10.1029/TC002i001p00063>.
- Rubatto, D., Hermann, J., 2007. Experimental zircon/melt and zircon/garnet trace element partitioning and implications for the geochronology of crustal rocks. *Chem. Geol.* 241, 38–61. <https://doi.org/10.1016/j.chemgeo.2007.01.027>.
- Rudinec, R., 1989. *Nový pohľad na paleogeografický vývoj transkarpátskej depresie v neogéne* (New view onto the paleogeographic development of the Transcarpathian depression during the Neogene; In Slovak, Engl. abstract). *Miner. Slov.* 21, 27–42.
- Salteras, V.J.M., Hart, S.R., Pantó, Gy, 1988. Origin of Late Cenozoic volcanic rocks of the Carpathian arc, Hungary. In: Royden, L., Horváth, F. (Eds.) *The Pannonian Basin. A study in basin evolution*. *Am. Assoc. Pet. Geol. Mem.*, 279–292. doi:10.1306/m45474c19.
- Saunders, K.E., Morgan, D.J., Baker, J.A., Wysoczanski, R.J., 2010. The magmatic evolution of the Whakamaru supereruption, New Zealand, constrained by a microanalytical study of plagioclase and quartz. *J. Petrol.* 51, 2465–2488. <https://doi.org/10.1093/ptology/egq064>.
- Schärer, U., 1984. The effect of initial ^{230}Th disequilibrium on young UPb ages: the Makalu case, Himalaya. *Earth Planet. Sc. Lett.* 67, 191–204. [https://doi.org/10.1016/0012-821X\(84\)90114-6](https://doi.org/10.1016/0012-821X(84)90114-6).
- Schmid, S.M., Bernoulli, D., Fügenschuh, B., Matenco, L., Schefer, S., Schuster, R., Tischler, M., Ustaszewski, K., 2008. The Alpine-Carpathian-Dinaridic orogenic system: correlation and evolution of tectonic units. *Swiss J. Geosci.* 101, 139–183. <https://doi.org/10.1007/s00015-008-1247-3>.
- Seghedi, I., Downes, H., Harangi, S., Mason, P.R.D., Pécskay, Z., 2005. Geochemical response of magmas to Neogene-Quaternary continental collision in the Carpathian-Pannonian region: A review. *Tectonophysics* 410, 485–499. <https://doi.org/10.1016/j.tecto.2004.09.015>.
- Seghedi, I., Besutiu, L., Mirea, V., Zlănean, L., Popa, R.-G., Szakács, A., Atanasii, L., Pomeran, M., Vişan, M., 2019. Tectono-magmatic characteristics of post-collisional magmatism: Case study East Carpathians, Călimani-Gurghiu-Harghita volcanic range. *Phys. Earth Planet.* 293. <https://doi.org/10.1016/j.pepi.2019.106270>
- Seghedi, I., Downes, H., 2011. Geochemistry and tectonic development of Cenozoic magmatism in the Carpathian-Pannonian region. *Gondw. Res.* 20, 655–672. <https://doi.org/10.1016/j.jgr.2011.06.009>.
- Seghedi, I., Balintoni, I., Szakács, A., 1998. Interplay of tectonics and neogene post-collisional magmatism in the intracarpathian region. *Lithos* 45, 483–497. [https://doi.org/10.1016/S0024-4937\(98\)00046-2](https://doi.org/10.1016/S0024-4937(98)00046-2).
- Seghedi, I., Downes, H., Pécskay, Z., Thirlwall, M.F., Szakács, A., Prychodko, M., Matthey, D., 2001. Magmagenesis in a subduction-related post-collisional volcanic arc segment: the Ukrainian Carpathians. *Lithos* 57, 237–262. [https://doi.org/10.1016/S0024-4937\(01\)00042-1](https://doi.org/10.1016/S0024-4937(01)00042-1).
- Seghedi, I., Downes, H., Szakács, A., Mason, P.R.D., Thirlwall, M.F., Roşu, E., Pécskay, Z., Márton, E., Panaiotu, C., 2004. Neogene-Quaternary magmatism and geodynamics in the Carpathian-Pannonian region: a synthesis. *Lithos* 72, 117–146. <https://doi.org/10.1016/j.lithos.2003.08.006>.
- Seghedi, I., Ntaflous, T., Pécskay, Z., 2008. *The Gataia Pliocene lamproite: a new occurrence at the southeastern edge of the Pannonian Basin, Romania*. *Geol. Soc., London Spec. Publ.* 293, 83–100.
- Seghedi, I., Maţencu, L., Downes, H., Mason, P.R.D., Szakács, A., Pécskay, Z., 2011. Tectonic significance of changes in post-subduction Pliocene-Quaternary magmatism in the south east part of the Carpathian-Pannonian Region. *Tectonophysics* 502, 146–157. <https://doi.org/10.1016/j.tecto.2009.12.003>.
- Seghedi, I., Ersoy, Y.E., Helvacı, C., 2013. Miocene-Quaternary volcanism and geodynamic evolution in the Pannonian Basin and the Menderes Massif: A comparative study. *Lithos* 180–181, 25–42. <https://doi.org/10.1016/j.lithos.2013.08.017>.
- Seghedi, I., Lukács, R., Soós, I., Guillong, M., Bachmann, O., Cserép, B., Harangi, S., 2023. Magma evolution in a complex geodynamic setting, South Harghita volcanic area, East-Central Europe: Constraints from magma compositions and zircon petrochronology. *Lithos* 442–443. <https://doi.org/10.1016/j.lithos.2023.107059>
- Šegvić, B., Lukács, R., Mandic, O., Strauss, P., Badurina, L., Guillong, M., Harzhauser, M., 2023. U-Pb zircon age and mineralogy of the St Georgen haloysite tuff shed light on the timing of the middle Badenian (mid-Langhian) transgression, ash dispersal and palaeoenvironmental conditions in the southern Vienna Basin, Austria. *J. Geol. Soc.* 180. <https://doi.org/10.1144/jgs2022-106>.
- Self, S., 2006. The effects and consequences of very large explosive volcanic eruptions. *Philos. T. R. Soc. A* 364, 2073–2097. <https://doi.org/10.1098/rsta.2006.1814>.

- Simon, J.L., Reid, M.R., 2005. The pace of rhyolite differentiation and storage in an 'archetypical' silicic magma system, Long Valley, California. *Earth Planet. Sc. Lett.* 235, 123–140. <https://doi.org/10.1016/j.epsl.2005.03.013>.
- Sláma, J., Košler, J., Condon, D.J., Crowley, J.L., Gerdes, A., Hanchar, J.M., Horstwood, M.S.A., Morris, G.A., Nasdala, L., Norberg, N., Schaltegger, U., Schoene, B., Tubrett, M.N., Whitehouse, M.J., 2008. Plešovice zircon – A new natural reference material for U-Pb and Hf isotopic microanalysis. *Chem. Geol.* 249, 1–35. <https://doi.org/10.1016/j.chemgeo.2007.11.005>.
- Śliwiński, M., Babel, M., Nejbort, K., Olszewska-Nejbort, D., Gąsiewicz, A., Schreiber, B.C., Benowitz, J.A., Layer, P., 2012. Badenian-Sarmatian chronostratigraphy in the Polish Carpathian Foredeep. *Palaeogeog. Palaeoclimatol. Palaeoecol.* 326–328, 12–29. <https://doi.org/10.1016/j.palaeo.2011.12.018>.
- Sliwinski, J.T., Guillong, M., Liebske, C., Dunkl, I., von Quadt, A., Bachmann, O., 2017. Improved accuracy of LA-ICP-MS U-Pb ages of Cenozoic zircons by alpha dose correction. *Chem. Geol.* 472, 8–21. <https://doi.org/10.1016/j.chemgeo.2017.09.014>.
- Sliwinski, J.T., Guillong, M., Horstwood, M.S.A., Bachmann, O., 2022. Quantifying long-term reproducibility of zircon reference materials by U-Pb LA-ICP-MS dating. *Geostand. Geoanal. Res.* 46, 401–409. <https://doi.org/10.1111/ggr.12442>.
- Söderlund, U., Patchett, P.J., Vervoort, J.D., Isachsen, C.E., 2004. The ^{176}Lu decay constant determined by Lu-Hf and U-Pb isotope systematics of Precambrian mafic intrusions. *Earth Planet. Sc. Lett.* 219, 311–324. [https://doi.org/10.1016/S0012-821X\(04\)00012-3](https://doi.org/10.1016/S0012-821X(04)00012-3).
- Soták, J., Biroň, A., Prokešova, R., Spišák, J., 2000. Detachment control of core complex exhumation and back-arc extension: case study from East Slovak basin. *Geolines* 10, 66–67.
- Sparks, S., Self, S., Grattan, J., Oppenheimer, C., Pyle, D., Rymer, H., 2005. *Super-eruptions: global effects and future threats. Report of a Geological Society of London Working Group.*
- Stelten, M.E., Cooper, K.F., Vazquez, J.A., Calvert, A.T., Glessner, J.J.G., 2015. Mechanisms and timescales of generating eruptible rhyolitic magmas at Yellowstone Caldera from zircon and sanidine geochronology and geochemistry. *J. Petrol.* 56, 1607–1642. <https://doi.org/10.1093/ptrology/egv047>.
- Subová, V., Rybár, S., Šarinová, K., Hudáčková, N., Jamrich, M., Sliva, L., Šály, B., Hlavatý, I., 2022. Evolution of the lower Badenian depositional system in the East Slovakian Basin: Implications for reservoir rock potential. *Geol. Carpath.* 73, 319–352. <https://doi.org/10.31577/GeolCarp.73.4.3>.
- Sun, S.-S., McDonough, W.F., 1989. Chemical and isotopic systematics of oceanic basalts: implications for mantle composition and processes. *Geol. Soc., London Spec. Pub.* 42, 313–345. <https://doi.org/10.1144/GSL.SP.1989.042.01.19>.
- Swallow, E.J., Wilson, C.J.N., Charlier, B.L.A., Gamble, J.A., 2019. The Huckleberry Ridge Tuff, Yellowstone: evacuation of multiple magmatic systems in a complex episodic eruption. *J. Petrol.* 60, 1371–1426. <https://doi.org/10.1093/ptrology/egz034>.
- Szabó, C., Harangi, S., Csontos, L., 1992. Review of Neogene and Quaternary volcanism of the Carpathian-Pannonian region. *Tectonophysics* 208, 243–256. [https://doi.org/10.1016/0040-1951\(92\)90347-9](https://doi.org/10.1016/0040-1951(92)90347-9).
- Széky-Fux, V., Kozák, M., 1984. A Nyírség mélyszintű neogén vulkanizmusa. *Földt. Közl.* 114, 147–159.
- Szentgyörgyi, K., 1978. The Sarmatian formations in the Tiszántúl area (East Hungary) and their stratigraphic position. *Acta Miner.-Petrogr.* 23, 279–297.
- Szepesti, J., Lukács, R., Soós, I., Benkó, Z., Pécskay, Z., Ésik, Z., Kozák, M., Di Capua, A., Gropelli, G., Norini, G., Sulpizio, R., Harangi, S., 2019. Telkibánya lava domes: Lithofacies architecture of a Miocene rhyolite field (Tokaj Mountains, Carpathian-Pannonian region, Hungary). *J. Volcanol. Geoth. Res.* 385, 179–197. <https://doi.org/10.1016/j.jvolgeores.2019.07.002>.
- Takarada, S., Hoshizumi, H., 2020. Distribution and eruptive volume of Aso-4 pyroclastic density current and tephra fall deposits, Japan: A M8 super-eruption. *Front. Earth. Sci.* 8. <https://doi.org/10.3389/feart.2020.00170>.
- Tărăpoancă, M., Garcia-Castellanos, D., Bertotti, G., Matenco, L., Cloetingh, S., Dinu, C., 2004. Role of the 3D distributions of load and lithospheric strength in orogenic arcs: Poly-stage subsidence in the Carpathians foredeep. *Earth Planet. Sc. Lett.* 221, 163–180. [https://doi.org/10.1016/S0012-821X\(04\)00068-8](https://doi.org/10.1016/S0012-821X(04)00068-8).
- Tari, G., Dövényi, P., Dunkl, I., Horváth, F., Lenkey, L., Stefanescu, M., Szafián, P., Tóth, T., 1999. Lithospheric structure of the Pannonian basin derived from seismic, gravity and geothermal data. In: Durand, B., Jolivet, L., Horváth, F., Séranne, M. (Eds.): *The Mediterranean Basins: Tertiary extension within Alpine Orogen.* *Geol. Soc., London, Spec. Pub.* 156: 215–250. doi:10.1144/gsl.sp.1999.156.01.12.
- Tari, G., Horváth, F., Rümpler, J., 1992. Styles of extension in the Pannonian Basin. *Tectonophysics* 208, 203–219. [https://doi.org/10.1016/0040-1951\(92\)90345-7](https://doi.org/10.1016/0040-1951(92)90345-7).
- Tari, G., Bada, G., Beidinger, A., Cszizmeg, J., Danišik, M., Gjerazi, I., Grasemann, B., Kováč, M., Plašienka, D., Šujan, M., Szafián, P., 2021. The connection between the Alps and the Carpathians beneath the Pannonian Basin: Selective reactivation of Alpine nappe contacts during Miocene extension. *Global Planet. Change* 197. <https://doi.org/10.1016/j.gloplacha.2020.103401>.
- Tuttle, O.F., Bowen, N.L., 1958. Origin of Granite in the Light of Experimental Studies in the System $\text{NaAlSi}_3\text{O}_8$ – KAlSi_3O_8 – SiO_2 – H_2O . *Geol. Soc. Am. Mem.* 74. <https://doi.org/10.1130/MEM74>.
- Ustaszewski, K., Schmid, S.M., Fügenschuh, B., Tischler, M., Kissling, E., Spakman, W., 2008. A map-view restoration of the Alpine-Carpathian-Dinaridic system for the Early Miocene. *Swiss J. Geosci.* 101, 273–294. <https://doi.org/10.1007/s00015-008-1288-7>.
- Ustaszewski, K., Kounov, A., Schmid, S.M., Schaltegger, U., Krenn, E., Frank, W., Fügenschuh, B., 2010. Evolution of the Adria-Europe plate boundary in the northern Dinarides: From continent-continent collision to back-arc extension. *Tectonics* 29. <https://doi.org/10.1029/2010TC002668>.
- Vasiliev, I., de Leeuw, A., Filipescu, S., Krijgsman, W., Kuiper, K., Stoica, M., Briceag, A., 2010. The age of the Sarmatian-Pannonian transition in the Transylvanian Basin (Central Paratethys). *Palaeog. Palaeoclimatol. Palaeoecol.* 297, 54–69. <https://doi.org/10.1016/j.palaeo.2010.07.015>.
- Vass, D., 1998. In: Rakús, M. (Ed.). *Geol. Surv. SR Dionýz Štúr Bratislava*, 115–188.
- Vass, D., Pereszlényi, M., Soták, J., Pipík, R., 2005. *Geology of the East Slovakian Basin. The State Geological Institute of Dionýz Štúr, Bratislava*, pp. 1–65.
- Vazquez, J.A., Reid, M.R., 2002. Time scales of magma storage and differentiation of voluminous high-silica rhyolites at Yellowstone caldera, Wyoming. *Contrib. Mineral. Petrol.* 144, 274–285. <https://doi.org/10.1007/s00410-002-0400-7>.
- Vazquez, J.A., Reid, M.R., 2004. Probing the accumulation history of the voluminous Toba Magma. *Science* 305, 991–994. <https://doi.org/10.1126/science.1096994>.
- von Quadt, A., Wotzlaw, J.-F., Buret, Y., Large, S.J.E., Peytcheva, I., Trinquier, A., 2016. High-precision zircon U/Pb geochronology by ID-TIMS using new 1013 ohm resistors. *J. Anal. Atom. Spectrom.* 31, 658–665. <https://doi.org/10.1039/C5JA00457H>.
- Watson, E.B., Harrison, T.M., 1983. Zircon saturation revisited: temperature and composition effects in a variety of crustal magma types. *Earth Planet. Sc. Lett.* 64, 295–304. [https://doi.org/10.1016/0012-821X\(83\)90211-X](https://doi.org/10.1016/0012-821X(83)90211-X).
- Wendt, I., Carl, C., 1991. The statistical distribution of the mean squared weighted deviation. *Chem. Geol. Isot. Geosci. Section* 86 (4), 275–285.
- Westgate, J.A., Pearce, N.J.G., Perkins, W.T., Preece, S.J., Chesner, C.A., Muhammad, R. F., 2013. Tephrochronology of the Toba tuffs: four primary glass populations define the 75-ka Youngest Toba Tuff, northern Sumatra, Indonesia. *J. Quaternary Sci.* 28, 772–776. <https://doi.org/10.1002/jqs.2672>.
- Wiedenbeck, M., Allé, P., Corfu, F., Griffin, W.L., Meier, M., Oberli, F., Quadt, A.V., Roddick, J.C., Spiegel, W., 1995. Three natural zircon standards for U-Th-Pb, Lu-Hf, trace element and ree analyses. *Geostand. Newslett.* 19, 1–23. <https://doi.org/10.1111/j.1751-908X.1995.tb00147.x>.
- Wilson, C.J.N., Rowland, J.V., 2016. The volcanic, magmatic and tectonic setting of the Taupo Volcanic Zone, New Zealand, reviewed from a geothermal perspective. *Geothermics*. 59, Part B, 168–187. <https://doi.org/10.1016/j.geothermics.2015.06.013>.
- Wilson, C.J.N., Cooper, G.F., Chamberlain, K.J., Barker, S.J., Myers, M.L., Illsley-Kemp, F., Farrell, J., 2021. No single model for supersized eruptions and their magma bodies. *Nat. Rev. Earth Environ.* 2, 610–627. <https://doi.org/10.1038/s43017-021-00191-7>.
- Woo, G., 1999. *The Mathematics of Natural Catastrophes.* Imperial College Press, London, pp. 1–292.
- Woodhead, J.D., Hergt, J.M., 2005. A preliminary appraisal of seven natural zircon reference materials for in situ Hf isotope determination. *Geostand. Geoanal. Res.* 29, 183–195. <https://doi.org/10.1111/j.1751-908X.2005.tb00891.x>.
- Wortel, M.J.R., Spakman, W., 2000. Subduction and slab detachment in the Mediterranean-Carpathian Region. *Science* 290, 1910–1917. <https://doi.org/10.1126/science.290.5498.1910>.
- Wu, F.-Y., Yang, Y.-H., Xie, L.-W., Yang, J.-H., Xu, P., 2006. Hf isotopic compositions of the standard zircons and baddeleyites used in U-Pb geochronology. *Chem. Geol.* 234, 105–126. <https://doi.org/10.1016/j.chemgeo.2006.05.003>.
- Zelenka, T., 1964. A Szerencsi-öböl szarmata tufaszintjei és fáciesei. *Földt. Közl.* 117, 237–253.
- Zelenka, T., Gyarmati, P., Kiss, J., 2012. Paleovolcanic reconstruction in the Tokaj Mountains. *Cent. Europ. Geol.* 55, 49–83. <https://doi.org/10.1556/CEuGeol.55.2012.1.4>.